Petroleum Science 22 (2025) 4736–4752

Contents lists available at ScienceDirect

Petroleum Science

journal homepage: www.keaipublishing.com/en/journals/petroleum-science

Original Paper

An experimental study of huff-and-puff oil recovery for tight-tuff heavy oil reservoirs by synergistic with viscosity reducer and CO_2 utilizing online NMR technology

Hao Chen [a,b,c,d,*], Pei-Fu Xu [a,b,c], Yong-Xian Zhu [e], Jia-Yi Yu [f], Mei Zhang [f], Xian-Min Zhou [g], Ming-Cheng Ni [a,b,c], Yi Wu [a,b,c], Xi-Liang Liu [a,b,c]

[a] Hainan Institute of China University of Petroleum (Beijing), Sanya, 572000, Hainan, China
[b] State Key Laboratory of Petroleum Resources and Engineering, China University of Petroleum (Beijing), Beijing, 102249, China
[c] School of Safety and Ocean Engineering, China University of Petroleum (Beijing), Beijing, 102249, China
[d] PetroChina Research Institute of Petroleum Exploration and Development, Beijing, 100083, China
[e] PetroChina Tuha Oilfield Company, Hami, 838013, Xinjiang, China
[f] Research Institute of Exploration and Development, PetroChina Oilfield Company, Hami, 839009, Xinjiang, China
[g] Acrocean Sci & Tech Development LLC, Houston TX 77433, USA

ARTICLE INFO

Article history:
Received 1 November 2024
Received in revised form
29 July 2025
Accepted 29 July 2025
Available online 7 August 2025

Edited by Yan-Hua Sun

Keywords:
Tight-tuff heavy oil reservoir
Reservoir rock and live oil
Low limit of pore utilization
CO_2 and HDC huff-and-puff
Online NMR
Improved oil recovery

ABSTRACT

The tight-tuff heavy oil reservoir exhibits severe heterogeneity and is characterized by high density, high viscosity, and a high wax content, posing significant challenges for its development. While CO_2 huff-and-puff (H-n-P) enhances oil recovery, these reservoirs struggle with low displacement efficiency. This study proposes a method that combines CO_2 with an oil-soluble viscosity reducer to improve displacement efficiency in the H-n-P process for tight-tuff heavy oil reservoirs. It also focuses on evaluating pore utilization limits and optimizing the injection strategy. Core samples and crude oil from the TH oilfield (a tight-tuff heavy oil reservoir) were used to conduct online NMR core flooding experiments, including depletion development, water, CO_2, and HDC (CO_2 combined with an oil-soluble viscosity reducer) H-n-P injection processes. A single-porosity model accurately reflecting its geological characteristics was developed using the GEM component simulator within the CMG numerical simulation software to investigate the optimized schemes and the enhanced oil recovery potential for a tight-tuff heavy oil reservoir in the TH oilfield. This model was utilized to evaluate the impact of various injection strategies on oilfield recovery efficiency. The study was designed and implemented with five distinct injection schemes.

Results showed that oil was produced primarily from large and medium pores during the depletion stage, while water H-n-P, with CO_2 H-n-P, first targeted macropores, then mesopores, and micropores. The lower pore utilization limit was 0.0267 μm. In the HDC H-n-P process, most oil was recovered from water-flooded pores. Still, HDC's lower injection capacity increased the pore utilization limit to 0.03 μm, making micropore recovery difficult. Experimental and modeling results suggest that the optimal development plan for the TH oilfield is one cycle of HDC H-n-P followed by two cycles of CO_2 H-n-P. This strategy leverages HDC's ability to promote water and oil recovery in the early stage and mass transfer and extraction capacity of CO_2 in later cycles.

Additionally, the characteristics of CO_2 and HDC H-n-P processes, pore utilization, and recoverable oil (at the pore scale) were evaluated. The results of this study are crucial for refining the reservoir development plan.

* Corresponding author.
E-mail address: chenhaomailbox@163.com (H. Chen).

Peer review under the responsibility of China University of Petroleum (Beijing).

https://doi.org/10.1016/j.petsci.2025.07.021

1. Introduction

The tight sedimentary tuff reservoir of the Permian Tiaohu Formation in the Santanghu Basin represents the first successful exploration and development of a tuff-type tight reservoir in China and globally (Li A. et al., 2015; Liang et al., 2019; Yu et al., 2020). The reservoir is characterized by medium to high porosity, ultra-low permeability, a high oil saturation of 69.1%, crude oil density ranging from 0.89 to 0.91 g/cm^3, high oil viscosity, and a high wax content, making production challenging. While horizontal wells with volume fracturing technology have enabled overall reserve production, production has decreased due to low oil recovery factors for primary, and poor performance persists. To address these issues, two technologies, the seam network overlaps in the small well-spacing and water flooding with imbibition in the well group, have temporarily resolved such issues and increased oil recovery from 2.5% to 10.2%. However, challenges remain regarding the next steps for future development.

Carbon dioxide is acknowledged as a significant factor in the rising levels of atmospheric carbon (Li et al., 2021; Ren et al., 2021; Xu et al., 2021; Xia et al., 2024). In recent years, researchers have conducted numerous studies aimed at reducing carbon dioxide emissions and investigating the viability of underground carbon dioxide storage. Carbon dioxide flooding has been proven to be a pivotal strategy for enhancing the recovery efficiency of tight reservoirs. This technique induces various oil displacement mechanisms under different environmental conditions: (1) In low-pressure settings, it acts by expanding crude oil, diminishing oil viscosity, enhancing fluid mobility ratios, improving reservoir permeability, and facilitating solvent gas flooding (Luo et al., 2023a; Wang L. et al., 2023; Yan et al., 2025; Zhou et al., 2024a, 2024b). (2) In moderate pressure settings, carbon dioxide initiates the extraction of lighter components from crude oil, with the quantity of oil extracted by carbon dioxide increasing with pressure (Kumar et al., 2022; Lu et al., 2024; Shi et al., 2024; Wang et al., 2023). (3) Under high-pressure conditions, the ability of carbon dioxide to extract and gasify crude oil is greatly increased, rapidly forming a miscible phase near the wellbore (Huang et al., 2023; Ordorica-Garcia et al., 2009; Tang et al., 2024; Wu et al., 2020). (4) Other notable characteristics include its low viscosity and high diffusion coefficient, which can effectively initiate crude oil within tight pores (Davoodi et al., 2024; Du et al., 2023; Luo et al., 2023b; Moultos et al., 2016; Sun et al., 2023). The characteristics of the reservoir environment dictate the dominance of each mechanism. For instance, reducing crude oil viscosity with carbon dioxide is especially important in heavy oil reservoirs. In light oil reservoirs with lower pressure, carbon dioxide plays a crucial role in enhancing the swelling of crude oil. In reservoirs with high water cuts, carbon dioxide exerts a more significant positive effect on diminishing inter-fluid mobility than overall reservoir development. By aligning the development strategy with the attributes of the reservoir environment, the exploitation of tight oil reservoirs via carbon dioxide can be optimized to achieve maximum efficacy (Alcalde et al., 2021; Li et al., 2021; Song et al., 2020). However, the efficacy of solitary carbon dioxide flooding in developing certain unconventional reservoirs is not particularly effective. For instance, in some extremely low permeability, highly viscous, and highly heterogeneous reservoirs, its mobility may be constrained even if carbon dioxide can be injected. The formation of effective miscibility between CO_2 and crude oil may not be achieved, which increases the risk of gas channeling during carbon dioxide flooding and reduces the efficiency of the flooding process. The substantial costs associated with capturing, transporting, and injecting carbon dioxide contribute to unfavorable economics, thereby limiting the broad application of this technology.

In light of these challenges, a range of research has focused on scrutinizing the efficacy of viscosity-reducing agents (VRAs) in exploiting tight oil reservoirs. The principal objective of employing VRAs is to alter the molecular architecture of in-situ crude oil, thereby diminishing its viscosity and augmenting fluid mobility, which is pivotal for enhancing the recovery factor of tight oil deposits (Li et al., 2024; Liu et al., 2025; Lv et al., 2023; Sahu et al., 2023; Wang et al., 2025; Xu et al., 2022). Prominent oilfields, such as the Zhongyuan, Tahe, and Shengli oilfields, have successfully leveraged the injection of chemical VRAs to substantially improve the downstream conditions of reservoirs, thereby enhancing fluid mobility ratios and rock wettability, and consequently bolstering oil recovery rates. However, during extensive development and application, several drawbacks have emerged. The production costs associated with VRAs are notably high, and their performance can be inconsistent. Certain VRAs may interact with subsurface minerals, triggering corrosion and obstruction of production facilities. Moreover, there are instances where VRAs can emulsify crude oil and water, escalating the complexity of oil–water separation processes and potentially leading to diminished oil recovery (Liu et al., 2023; Tao et al., 2022; Wu et al., 2024; Zhao et al., 2021). Consequently, the contemplation of chemical VRAs must encompass an evaluation of their environmental ramifications, economic viability, technical practicability, and long-term sustainability. To mitigate these issues, future developments should focus on crafting VRAs that are cost-effective, stable, and compatible with subsurface conditions, without compromising the integrity of production equipment or complicating the separation processes.

The production of the tight-tuff reservoirs is highly dependent on the reservoir's relative permeability, the oil viscosity, the reservoir wettability, and the formation volume of the target formation. Considering the unique characteristics of the formation and fluids in this type of reservoirs, achieving effective production solely through carbon dioxide injection or viscosity reducers is challenging. In recent years, HDC (CO_2 combined with an oil-soluble viscosity reducer) flooding technology has demonstrated remarkable applications in heavy oil reservoirs with medium to high permeability, such as the Chenjiazhuang Formation of Shengli Oilfield and the Xingbei Formation of Taizhou in the East China Oilfield (Hao et al., 2022; Ozkan et al., 2012; Wei et al., 2020). For instance, one well's daily oil production increased from 0.1 to 8–14.95 tons, while the water cut dropped from 99% to 7%–11%, significantly improving oil production performance. This technique's mechanisms include the following: 1) Horizontal wells are used to increase gas injection capacity and discharge area of oil in the formation, improve the production dynamics of recoverable oil in the horizontal direction, and prolong the time of low water cuts. 2) In the early stage of a target reservoir, a viscosity reducer is injected to effectively disperse and break down colloidal-asphaltene aggregates, significantly reducing the viscosity of formation oil. This enhances the subsequent dissolution capacity of carbon dioxide and clears blockages caused by the deposition of heavy components from CO_2 precipitation. 3) Subsequently, carbon dioxide is injected to carry the viscosity reducer, leading to the extension of the range of the viscosity reducer, activating multiple mechanisms of CO_2 displacing oil in the formation. This technology has primarily been applied to gas flooding in conventional heavy oil reservoirs.

However, the microscopic mechanisms at the micro-nanopore scale during the HDC huff-and-puff (H-n-P) injection in heavy oil formations after water injection remain unclear. It is uncertain whether viscosity reducers and carbon dioxide can work together synergistically, and the mechanisms and extent of oil recovery enhancement at different development stages are poorly understood. The utilization of a minimum pore size limit for oil recovery

in tight-tuff heavy oil reservoirs has not yet been determined. Therefore, this study proposes an optimal strategy for field implementation by analyzing three key parameters: oil recovery at the pore scale, oil change rate (efficiency of injecting carbon dioxide and HDC to displace crude oil), and the input-to-output ratio (investment in injection cost-to-benefit of production). The analysis focuses on the development characteristics and the utilization of a minimum limit of recoverable crude oil at the pore scale during CO_2 injection and HDC multi-cycle H-n-P after water injection in typical sedimentary tuff heavy oil reservoirs. To support this, laboratory physical experiments were conducted using an online nuclear magnetic resonance (NMR) core flooding technique.

2. Experimental

2.1. Experimental materials

2.1.1. Preparation for test samples

Cores #1 and #2 were collected from the target block in the tight-tuff heavy oil reservoirs and cut into cylindrical samples. A porosimeter, manufactured by Tuochuang Tech., Jiangsu, China, was utilized to measure the porosity of shale rock samples, following a methodology comparable to that described in the literature (Li et al., 2023). The TC-200 Pulse Decay Permeameter, manufactured by Tuochuang Tech., Jiangsu, China, was employed to determine the permeability of shale rock samples, adhering to a procedure outlined in the literature (Zhao et al., 2022). Based on the obtained porosity and permeability data, shale rock samples with similar porosity and permeability values were selected for CO_2 and HDC H-n-P injection experiments. Table 1 displays the dimensions of the core samples, which exhibit similar physical properties in terms of porosity and permeability.

Before running the injection experiment, the core end face was flattened using wire cutting to eliminate the gap between the core and the end plug in the core holder. The core sample was dried in an oven at 104 °C for 48 h to reach a constant dry weight. Filter paper was placed between two core samples for uniform fluid distribution (Bank et al., 2007; Cao and Gu, 2013; He et al., 2020; Huang et al., 2022; Jia, 2019). The core sample was encased in a heat-shrink tube to isolate the fluorinated solution, increase the confining pressure, and prevent CO_2 from entering the annular space. The fluorinated solution is a non-magnetic material. To avoid the interference of hydrogen signals caused by water injection, deuterium water (D_2O) was used as the injection agent for the water H-n-P injection experiment.

2.1.2. Experimental crude oil and gas

Surface crude oil and gas were taken from well X in the TH oilfield. The density and viscosity for such oil are 0.86 g/cm^3 and 43.51 mPa·s under reservoir conditions (65 °C, 25.6 MPa), respectively. The live oil used in this study was combined in the PVT laboratory based on the dissolved gas composition and gas–oil ratio of 18.70 m^3/m^3.

2.1.3. Displacing agents

CO_2 and N_2 are industrial gases with a purity of 99.99%, heavy water (D_2O) is 99.9 at%, and the density of D_2O is 1.107 g/cm^3. All of these are used as displacing agents for the H-n-P injection process.

Table 1
Dimensions and properties of reservoir cores.

Core ID	Length, cm	Diameter, cm	Porosity, %	Permeability, mD
Core #1	7.26	2.44	14.94	0.201
Core #2	7.13	2.45	15.39	0.224

2.1.4. Viscosity reducer

The viscosity reducer used in this study is an oil-soluble ternary polymer (1 wt%) developed during the initial screening phase. It was synthesized via copolymerization of maleate, vinyl acetate, and acrylamide. To evaluate its performance, three types of viscosity measurements were conducted: crude oil alone, viscosity reducer alone, and mixtures of CO_2 and the viscosity reducer at seven different mass ratios (6:1, 7:1, 8:1, 9:1, 10:1, 11:1, and 12:1), with the volume of crude oil kept constant in all cases. All viscosity measurements followed the equipment specifications and testing procedures outlined in the Natural Gas Industry Standard of the People's Republic of China (SY/T 5542-2009), and were performed under reservoir-simulated conditions of 65 °C and 32 MPa. Fig. 1 shows the viscosities of crude oil, viscosity reducer, and CO_2–reducer mixtures at various ratios, as well as their effectiveness in reducing crude oil viscosity.

Under experimental conditions, the viscosities of the viscosity reducer and crude oil are 17.53 and 43.52 mPa·s, respectively. The difference in viscosities between them was 25.99 mPa·s. Under the experimental conditions, the viscosity reduction ratio peaked at 79.32% when the mass ratio of CO_2 to viscosity reducer was 9:1. Further increases in the CO_2-to-reducer ratio resulted in only marginal improvements, indicating diminishing returns. Therefore, a 9:1 mass ratio was selected as the optimal condition for the HDC H-n-P injection tests.

According to the testing results in Fig. 1, the viscosity of the mixture of CO_2, viscosity reducer, and crude oil significantly decreases. When CO_2 is added to the mixture of crude oil and viscosity reducer, the viscosity of such a mixture (the ratio of 6:1, as shown in Fig. 1) can be reduced compared to that of the mixture of crude oil and viscosity reducer. Decreased oil viscosity improves the oil flow and increases the relative permeability to the oil phase, which benefits CO_2-enhanced oil recovery. The swelling and dispersion effects of CO_2 can explain this phenomenon. As a result, the oil recovery can be improved, as proved by HDC H-n-P injection tests in this study.

2.2. Experimental device and procedure

2.2.1. Experimental device

The experimental device is a high-temperature (HT) and high-pressure (HP) H-n-P core flooding device independently developed in-house. It can withstand working pressures of up to 50 MPa and temperatures of up to 90 °C. The device consists of the following parts: an online NMR monitoring system, a MesoMR12-060H-I HT and HP NMR analyzer with core assembly, an HT and HP displacement pump, a back pressure regulator (BPR), and a gas

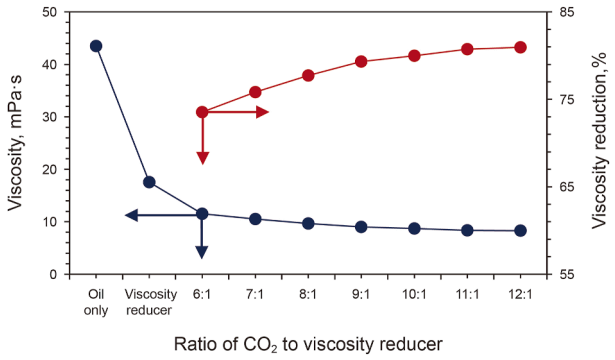

Fig. 1. Viscosity of CO_2–viscosity reducer mixtures and their viscosity reduction efficiency on crude oil at different CO_2-to-reducer ratios.

chromatograph (Suzhou Neway Analytical Instrument Co., Ltd., China), as shown in Fig. 2.

The NMR system is characterized by a magnetic field strength of 0.23±0.03 T and an imaging gradient peak intensity exceeding 3.5 G/cm. It supports fewer than 18,000 CPMG echoes, with a minimum echo time of less than 60 μs. The pulse frequency range is 1–30 MHz, with a frequency control accuracy of 0.1 Hz and a pulse timing accuracy of 100 ns. Imaging performance includes a signal-to-noise ratio of above 20 dB, image distortion of below 15%, and image uniformity of greater than 45%. The system can operate at temperatures of up to 150 °C. The displacement apparatus maintains stable confining pressure and temperature conditions for the core within the core holder by circulating a fluoride-based fluid. This setup ensures a temperature control error within ±0.5 °C, regulated by a confining pump. A high-precision back pressure regulator (BPR) combined with a displacement pump maintains a volume error of ±0.05 mL. The displacement pump supports multiple operating modes, including constant pressure and constant flow rate displacement.

2.2.2. Standardization of NMR signal and oil content in the test sample

Before the H-n-P experiment, the core samples were cleaned using a Soxhlet extractor for 30 days to remove residual hydrocarbons and impurities. To calibrate the NMR acquisition parameters, reference cores with pore and permeability characteristics similar to those of the experimental samples were selected. By saturating these reference cores with varying oil contents, the corresponding T_2 relaxation time distributions were obtained. The total NMR signal amplitude was calculated by integrating the T_2 spectra and compared with the actual oil content. When the deviation between the NMR-derived and actual oil saturation was less than 5%, the NMR operating parameters were considered to properly set. Considering the high porosity and ultra-low permeability of the tested cores, the NMR scanning parameters were set as follows: wait time of 1500 ms, echo time of 1.2 ms, 4096 echoes, and four signal accumulations.

2.2.3. Experimental procedure

After setting the operational parameters for the NMR apparatus, the experiment was started following the outline presented in Table 2, and the testing procedures were as follows: (1) The core, cleaned with petroleum ether, was placed in a vacuum oven and dried at 102 °C for 48 h to remove water molecules from the tight-tuff core sample. (2) Perform an NMR scan on the core sample to obtain the basic information of the tight-tuff core. (3) The core sample was sealed in a heat-shrink tube for fixation, and petroleum ether was injected to pressurize the sample up to 32 MPa to prevent degassing of the subsequent live oil. The sample was then heated to the experimental temperature of 65 °C. Live oil was injected at a constant pressure of 32 MPa to saturate the core until the produced oil-to-gas ratio stabilized, thereby completing the saturation process. (4) The test sample saturated with live oil was scanned for the initial T_2 signal, then depletion development was conducted. The pressure was reduced from 32 to 8 MPa in an interval of 4 MPa. An NMR signal scan was performed as the reservoir pressure dropped from 32 to 8 MPa. After depletion, heavy water (D_2O) was injected into the core sample, and then the pressure was increased back to 32 MPa, and then soaked for 12 h before the pressure was gradually reduced again to 8 MPa for the production "puff" (see sequence 4 in Table 2). (5) Inject CO_2 into the test sample to increase pressure up to 32 MPa. After a 12-h

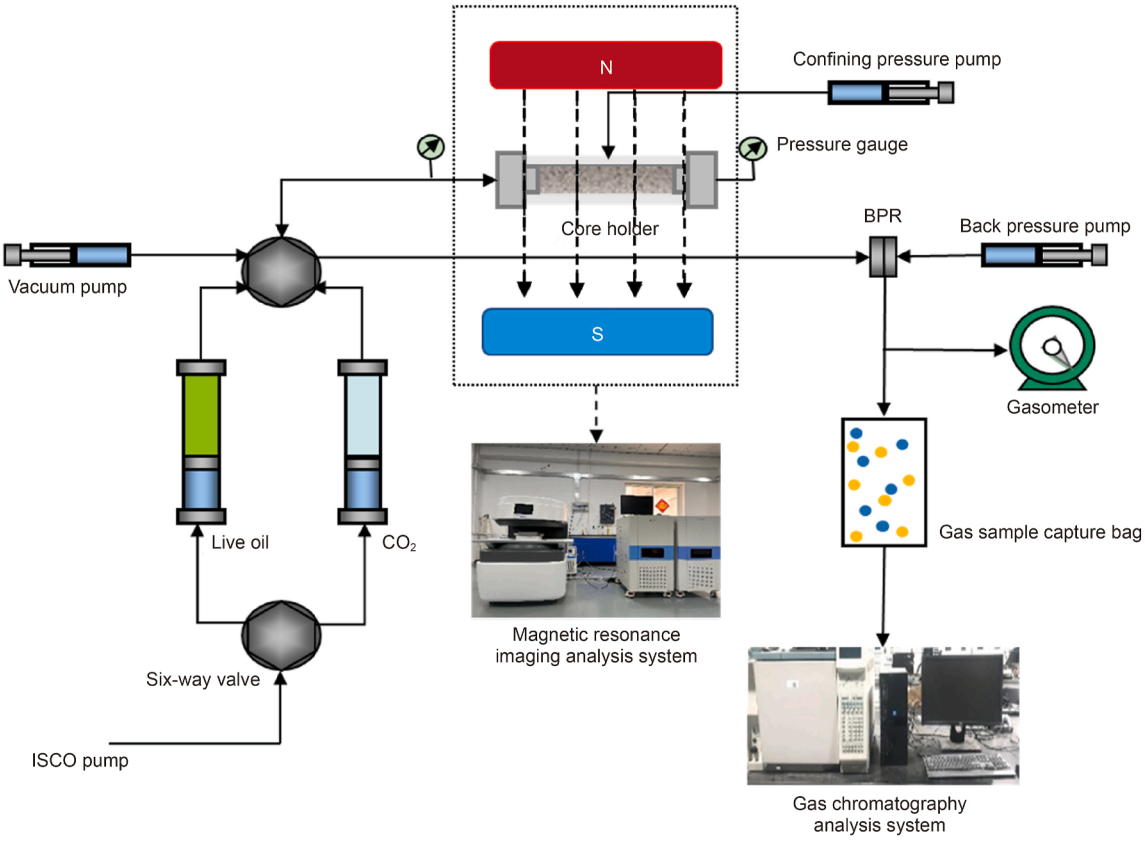

Fig. 2. Schematic diagram of the experimental setup for online NMR CO_2/HDC H-n-P tests.

Table 2
Outline of the experimental plan for the injection process.

Sequence	Task	Parameter setting	Displacing pattern
1	Improved pressure with petroleum ether	Increase the pressure to 32 MPa	Constant pressure displacement
2	Saturated core with live oil	GOR at the outlet of the core sample equals the original GOR	Constant pressure displacement
3	Depleted development	32 to 8 MPa	It decreases by every 4 MPa
4	Water H-n-P process	The pressure is increased to 32 MPa, maintained for 12 h, and then decreased to 8 MPa.	One cycle
5	CO_2/HDC H-n-P process	The pressure is increased to 32 MPa, maintained for 12 h, and then reduced to 8 MPa.	HDC, CO_2 plus viscosity reducer system, is pressurized to form a miscible phase and then injected into the core (When the pressure is greater than 16.9 MPa, the miscible phase is formed).

soaking period, the pressure was gradually reduced to 8 MPa (depleted pressure) until oil production ceases. (6) Use N_2 to clear the oil in the pipeline to reduce the error in the next test, repeat step (5), and carry out five cycles of the injection process.

For Core #2 (HDC scheme), steps (1)–(4) were performed. In step (5), the pre-configured mixture of CO_2 and 1 wt% oil-soluble viscosity reducer was injected into the test sample to reach 32 MPa. After soaking for 12 h, the pressure was gradually depleted to 8 MPa until no more oil was produced. Record all information required during this stage and perform the NMR scan again. After completing the HDC process, inject N_2 into the core to displace residual oil in the pipeline and minimize errors. These steps were repeated five times for the process.

2.2.4. Conversion of relaxation time and pore size

There are hydrogen nuclei in the formation fluid (crude oil or formation water) inside the pores of rocks. In the NMR experiment, the NMR signal amplitude and relaxation time T_2 of hydrogen nuclei in the fluid under the interaction of static magnetic field and applied magnetic field are measured, and T_2 spectra of different core samples are established (Chen et al., 2019; Or et al., 2016; Sayegh and Maini, 1984; Wei et al., 2020).

Through mercury injection and T_2 spectrum curves of core samples in different blocks, the relationship between the relaxation time spectrum and pore throat distribution of core samples is obtained, which is $y = 0.0583x^{0.3473}$ for this study. Fig. 3 represents an example of the fitting curve using mercury intrusion and relaxation time data. Fig. 3(a) shows the fitting curve between the relaxation time obtained from the NMR test and pore size distribution measured using the mercury injection test, and the conversion of the cumulative distribution frequency with relaxation time and pore size distribution in Fig. 3(b).

2.2.5. Characteristics of displacement efficiency by online NMR technology

Eq. (1) can calculate tight-tuff oil displacement efficiency or recovery before and after injection processes by utilizing online NMR technology. This approach quantifies tight-tuff oil recovery across different pore scales during experiments involving depleted development and water, CO_2, and HDC H-n-P injection processes. Oil recovery, as characterized by NMR technology, is defined as the ratio of the difference in area between the original T_2 spectrum distribution curve and the T_2 spectrum distribution curve at the end of each H-n-P injection process to the total area under the original T_2 spectrum distribution curve, which presents the original oil in place.

$$E_R = \left(1 - \frac{\int_{t_{min}}^{t_{max}} W_{H-n-P} dt}{\int_{t_{min}}^{t_{max}} W_i dt}\right) \times 100\% \quad (1)$$

where E_R represents the oil recovery factor at the pore scale; t_{max} denotes the maximum relaxation time with a certain pore size in the T_2 spectrum distribution, ms; t_{min} is the minimum relaxation time with a certain pore size in the T_2 spectrum distribution, ms; W_i is a function expression related to the signal intensity of the T_2 spectrum in the initial state of saturation with oil; $W_{H\text{-}n\text{-}P}$ represents a function expression related to the signal intensity of the T_2 spectrum after a certain cycle of the H-n-P injection process.

3. Results and discussion

3.1. Initial characterization of crude oil

Based on the distribution of saturated oil in the core shown in Fig. 4, the inflection points of the cumulative T_2 signal distribution curve are used to differentiate pore sizes within the core, which are classified into three categories: micropores (< 0.03 μm), mesopores (0.03–0.1 μm), and macropores (> 0.1 μm) (Gong et al., 2006; Hou et al., 2020; Li Z. et al., 2015; Luo et al., 2022; Tang et al., 2023; Timur, 1969). The average pore radii of the cores in this study were 0.019 μm for Core #1 and 0.025 μm for Core #2. After saturation with crude oil, the oil distribution in micropores, mesopores, and macropores was 14.81%, 63.24%, and 21.95% for Core #1 and 18.02%, 66.68%, and 15.30% for Core #2, indicating that the initial crude oil primarily accumulated in medium to large pores ranging from 0.03 to 0.1 μm.

The current findings on pore size distribution and oil saturation align with observations reported in the existing literature (Li et al., 2022; Li et al., 2024; Lu et al., 2021; Rylander et al., 2013). In these analyses, micropores, mesopores, and macropores are typically distinguished based on their T_2 relaxation times, which correlate with pore sizes. Rylander et al. (2013) reported a study of the Eagle Ford Shale that utilized NMR data to investigate pore size distribution and found that permeability to oil is influenced by pore throat size, wettability, and water saturation. The research revealed that larger pores significantly contribute to oil saturation, consistent with the observation that initial crude oil primarily accumulates in medium to large pores in this study (Rylander et al., 2013). Lu et al., 2021 employed an integrated analysis, including NMR, to investigate pore systems and fluid distribution in their research on the Eocene Shahejie Formation sandstone reservoirs. Their study emphasized the importance of understanding complex and heterogeneous pore structures to evaluate reservoir fluid distribution, resonating with the current approach of classifying pore sizes to assess oil

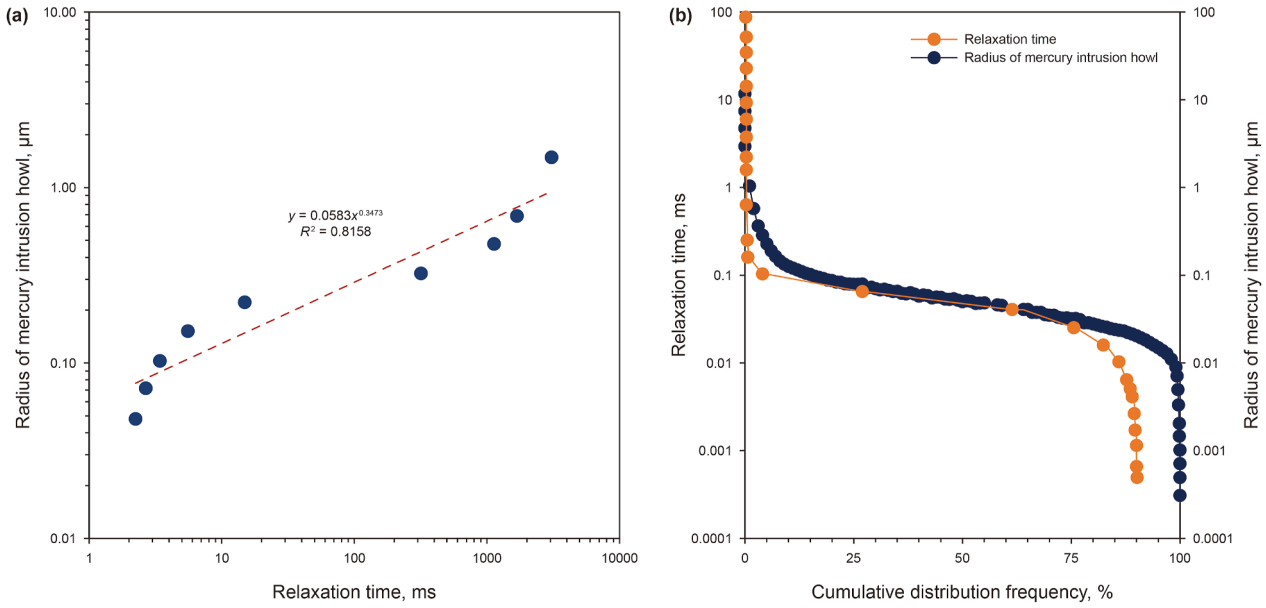

Fig. 3. Fitting of relaxation time and pore size distribution measured by the mercury intrusion method (**a**) and conversion (**b**).

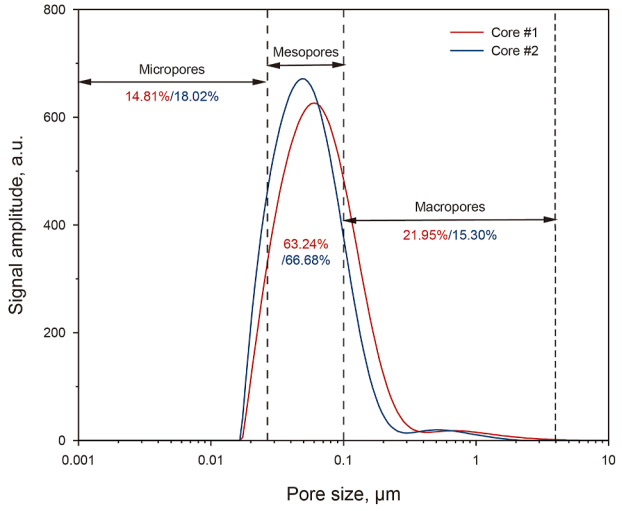

Fig. 4. Initial oil saturation distribution in Core #1 and Core #2.

distribution (Lu et al., 2021). The researchers (Li et al., 2022) employed 2D NMR to distinguish between different fluid components, such as free oil, bound oil, and water, within the pore structures of shale formations. Current findings, indicating that initial crude oil primarily accumulates in medium to large pores (0.03–0.1 μm), align with insights provided by 2D NMR analyses, which also emphasize the importance of understanding fluid occurrence states within various pore types to accurately assess hydrocarbon saturation and potential recoverability. Furthermore, shale core samples were subjected to oil saturation under 60 °C and 30 MPa. The oil saturation increased rapidly during the first 16 days and plateaued thereafter, reaching a maximum saturation of 46.2% after 20 days of vacuum and pressurization (Li et al., 2024).

3.2. Recoverable oil at pore scale during depletion development and water H-n-P injection stages

This study begins with the depletion development stage using natural energy, followed by a series of H-n-P injections with various displacing agents, as shown in Table 2. The T_2 spectrum signal in the depletion stage was first monitored to simulate the real development process. Several scans may be required to eliminate the influence of errors caused by fluctuations in the online nuclear magnetic scanning process. When the signal intensity difference between the two continuous scans for the core saturated with oil is greater than 5%, it indicates that the crude oil in the core pores has been recovered. Fig. 5(a) and (b) show the relationship between the NMR signal values and pore sizes of Core #1 and Core #2, respectively, for the cases of initial oil saturation and after the depleted development stage.

In the depleted development stage, the reservoir pressure, relying on the elastic energy of crude oil and reservoir rocks, declined, contributing to 95% of oil recovery in the macropores and mesopores. The lower limit of the pore size utilization related to oil production ranges from 0.019 to 0.020 μm, as shown in Fig. 5. Fig. 5 (a) and (b) reveal the case of Core #1 and Core #2, the recoverable oil with pore levels, respectively. The red curve shows a profile of the NMR signal value with pore size for the initial saturated oil in the core. The blue curve represents the profile of the NMR signal value with pore size at the reservoir pressure depleted to 8 MPa (elastic development period). The values show the percentage of the contribution of the recoverable oil in micropores, macropores, and mesopores, respectively. The majority of the oil produced was extracted from mesopores and macropores. Specifically, micropores contributed approximately 5.81% and 2.06% of the total oil production.

Compared with other research, the current findings align with existing literature on oil recovery mechanisms in low-permeability rocks. Wang et al. (2021) examined the water H-n-P process in low-permeability oil rocks and found that oil recovery is primarily enhanced through the supplementation of formation energy. The effectiveness of recovering oil using the water H-n-P process is more pronounced in larger pores due to better connectivity and lower capillary forces, resulting in higher oil recovery from mesopores and macropores (Wang et al., 2021). In another study, Zhang et al. (2023) investigated the microscopic production characteristics of crude oil. They found that high permeability, which correlates with larger pore sizes, results in better pore–throat connectivity and greater oil recovery. The study reported that small pores and macropores

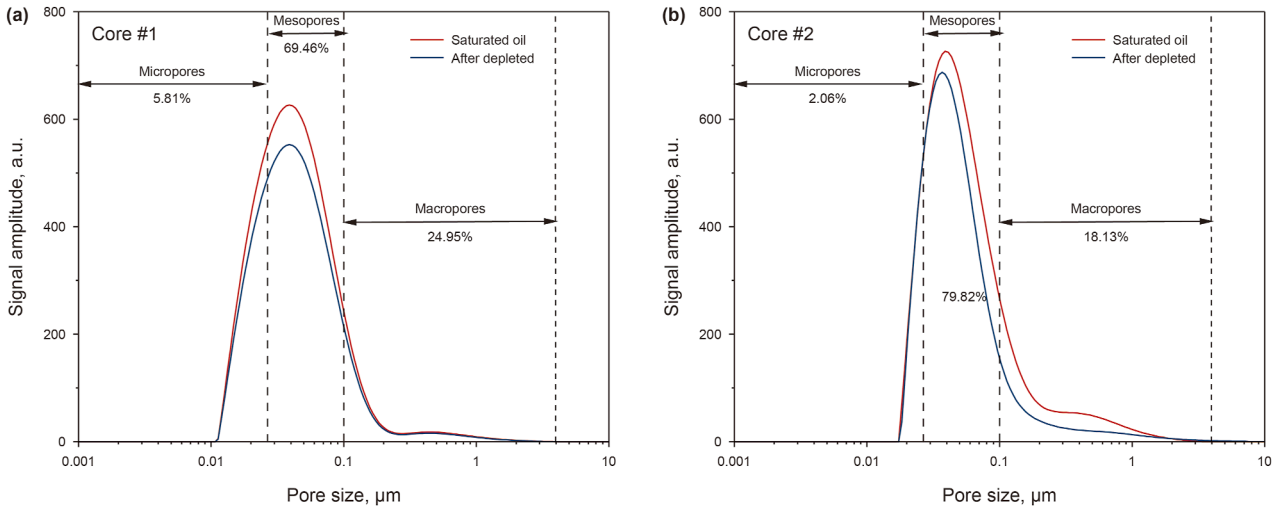

Fig. 5. T_2 spectra and recovered crude oil at the pore scale for Core #1 (**a**) and Core #2 (**b**) after the depletion development stage.

contribute significantly to oil production (Zhang et al., 2023). Furthermore, research by Li et al. (2023) explored the dynamic development characteristics of shale oil reservoir pores during depletion development. The study revealed that pore structure changes during development, with larger pores contributing more significantly to oil recovery due to their ability to maintain better connectivity and facilitate fluid flow (Li et al., 2023).

These studies support the current findings that depletion development and water H-n-P injection processes primarily recover oil from mesopores and macropores, with limited contribution from micropores and nanopores. The limited recovery from micropores is attributed to their poor connectivity and higher capillary forces, which impede fluid flow and oil displacement during extraction processes.

Based on the concept described in the depleted development stage, Fig. 6(a) and (b) show the T_2 spectrum profiles from the first cycle of the water (D_2O) huff (injection), soaking, and puff (production) process for Core #1 and Core #2, respectively. A significant leftward shift in the T_2 spectra of both cores was observed after the D_2O injection and soaking, indicating that the injected aqueous phase pushed crude oil from large and medium pores into the micropores, resulting in an increase in crude oil within the micropores, as shown in Fig. 7. Fig. 7(a) and (b) compare the remaining oil in Core #1 and Core #2 after depleted development and following the water H-n-P injection processes. It was observed that the remaining oil in both cores increased after the water H-n-P injection. Approximately 2.0% more oil was found in the micropores of both cores compared to the depleted development stage. During the production "puff" stage, crude oil is primarily recovered from the medium pores, contributing over 70% to recovery. The lower limit of the pore utilization remained at 0.0267 μm without decreasing.

Chen et al. (2018) investigated the effectiveness of water H-n-P in tight oil reservoirs. Utilizing NMR and magnetic resonance imaging (MRI), the fluid saturation, recovery rates, and residual oil distribution were monitored during core displacement processes. Their experiments revealed that over 80% of the pores in tight oil cores were sub-micro and micro-nanopores, with more than 77.8% of crude oil residing in these small pores. Movable fluids were primarily found in micropores with radii larger than 1 μm. Comparing these findings with the results of the current research, it was found that more than 77.8% of the crude oil existed in sub-

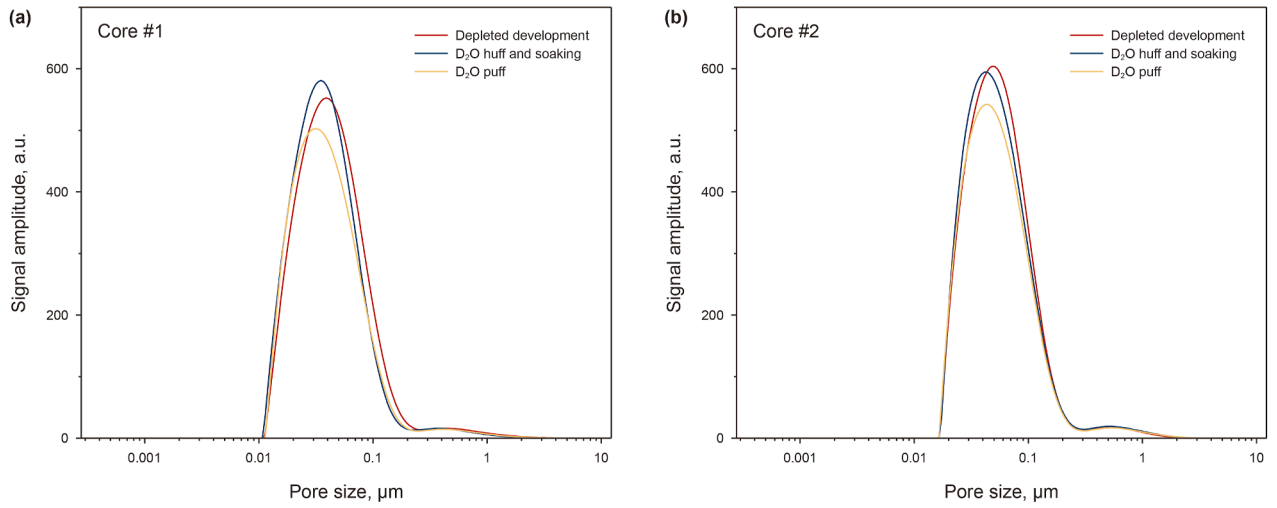

Fig. 6. T_2 spectrum vs. pore size distribution of water (D_2O) injection, huff, and puff for Core #1 (**a**) and Core #2 (**b**).

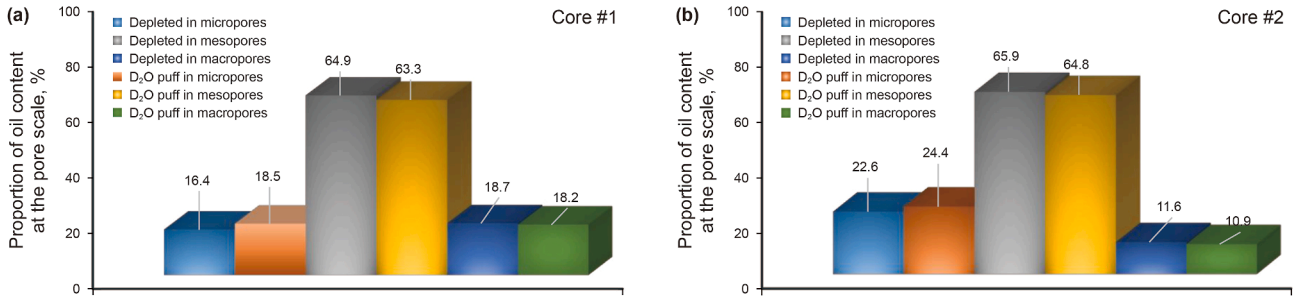

Fig. 7. Redistribution of oil saturation after water H-n-P injection process for Core #1 (**a**) and Core #2 (**b**).

micropores, with movable fluids mainly located in micropores larger than 1 μm (Chen et al., 2018).

In summary, this study highlights the effectiveness of water H-n-P injection in enhancing oil recovery in tight reservoirs. The findings offer further insights into the dynamic redistribution of oil across different pore sizes during the process. Understanding pore-scale fluid movements can inform optimization strategies for enhanced oil recovery in tight formations.

3.3. Assessment of oil extraction and displacement effectiveness during CO_2 and HDC H-n-P injection processes

The oil recovery performance of five cycles of CO_2 and HDC H-n-P injection processes on two depleted cores, which had undergone a depleted development stage and a water H-n-P injection scheme, was compared. The total oil recovery factor for the HDC process was higher (27.35%) than for CO_2 (20.30%). Most oil production occurred during the first two cycles, with similar recovery factors observed for the CO_2 H-n-P injection process in the last three cycles. For Core #2, using the HDC H-n-P injection process, oil recovery factors in cycles 3, 4, and 5 were comparable to those in the CO_2 H-n-P injection process.

Fig. 8 illustrates the changes in the lower limit of pore size utilized during the CO_2 and HDC H-n-P injection cycles. In Core #1, a noticeable shift in the lower limit of pore size utilization occurred during the first three CO_2 H-n-P injection process cycles. However, no such changes were observed in Core #2 for the HDC scheme. Regarding the lower limit of the pore utilization for Core #1 (Fig. 8(a)), the CO_2 H-n-P process reduced limit of pore size utilization from 0.0267 to 0.0194 μm by about 27% in the first two cycles and 45% after three cycles, reaching 0.0147 μm, which is based on the lower limit of pore size utilization of 0.0267 μm for mesopores. For Core #2 (Fig. 8(b)), the lower limit of pore size utilization during five cycles of HDC H-n-P remained near 0.0281 μm, reflecting an increase of about 5% to the end of the fifth cycle.

Similarly, the researchers investigated the CO_2 H-n-P-enhanced oil recovery mechanism and its influencing factors (Du et al., 2023). The research demonstrated that CO_2 H-n-P was superior to water flooding, showing an enhanced oil recovery performance advantage of about 15%. This study highlights the effectiveness of CO_2 H-n-P technology in unconventional oil and gas development and CO_2 storage (Du et al., 2023). Monger and Coma (1988) conducted a laboratory and field evaluation to investigate the use of cyclic CO_2 injection for enhanced recovery of light crude oil in rocks. Their results from core floods and 14 field tests indicated that cycles 1 and 2 were the most effective in enhancing oil recovery after water flooding. Factors such as larger reservoir slug volume, extended soak periods, thicker intervals, and lower prior water cut were identified as potential performance enhancers (Monger and Coma, 1988). Additionally, a review by Zhang et al. (2019) analyzed factors affecting CO_2 H-n-P recovery rates, emphasizing the impacts of permeability levels, fracture characteristics, and the number of H-n-P cycles on recovery efficiency. The study highlighted that while initial cycles are more productive, the efficiency declines in later cycles due to gas channeling and reservoir heterogeneity (Zhang et al., 2019).

In summary, CO_2 H-n-P injection processes demonstrated a total oil recovery factor of 20.30% after five cycles, with most oil production occurring during the first two cycles in this study. This trend is consistent with findings in existing literature, where initial cycles of CO_2 H-n-P yield higher recovery rates, followed by diminishing returns in subsequent cycles.

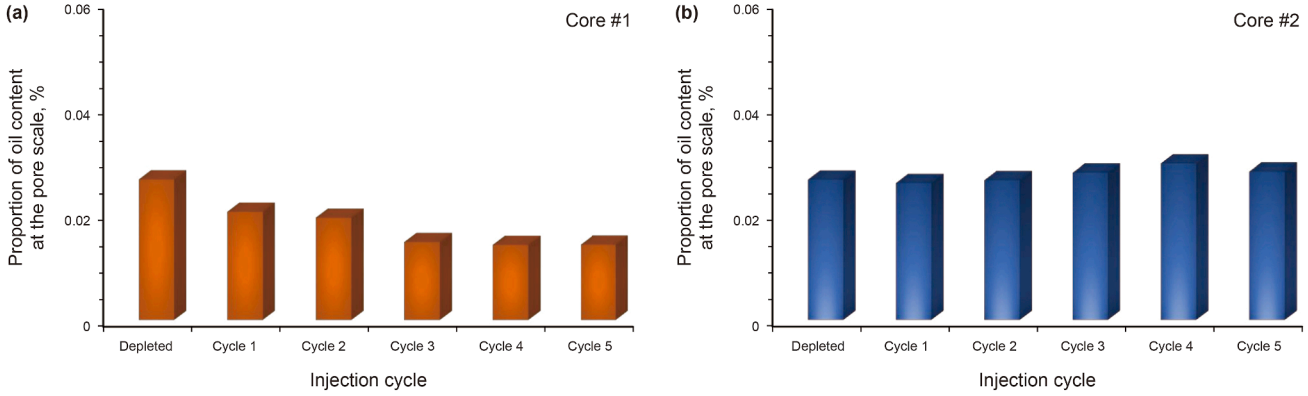

Fig. 8. Comparison of the lower limits of pore size utilization for CO_2 (Core #1) (**a**) and HDC (Core #2) (**b**) H-n-P injection processes after the depleted development stage and the water H-n-P injection process.

For the chemical-assisted CO_2 H-n-P injection process, Lu H. et al. (2021) proposed a novel enhanced oil recovery method developed using polymer gel-assisted CO_2 H-n-P to improve recovery in heavy oil reservoirs with high water cut through mobility control and selective plugging of high-permeability channels. The polymer gel, prepared using partially hydrolyzed polyacrylamide and other components, formed a special network structure to address reservoir heterogeneity. The study found that this method effectively enhanced oil recovery by improving the plugging effect and increasing the sweep efficiency of the CO_2 H-n-P process (Lu H. et al., 2021). Hao et al. (2022) investigated the use of a starch graft copolymer (SGC) gel to aid in the CO_2 H-n-P process. Laboratory experiments demonstrated that the SGC gel had better injectability and plugging ability than traditional polymer gels. Three-dimensional physical models with water channels revealed that four cycles of gel-assisted CO_2 H-n-P achieved an enhanced oil recovery of 11.36%, 2.56 times that of pure CO_2 H-n-P. Pilot tests further confirmed the economic benefits of this method in water-channeling reservoirs (Hao et al., 2022). Xia et al. (2024) proposed a method of surfactant slug (SC) assisting CO_2 H-n-P (SC-HNP) to address rapid production decline and poor development effects after volume fracturing of shale oil reservoirs through mechanisms of controlling CO_2 mobility, reducing IFT, and alternating wettability. Laboratory experiments and numerical simulations indicated that the SC-HNP method could significantly enhance oil recovery compared to the traditional CO_2 H-n-P process (Xia et al., 2024). Lv et al. (2024) introduced the $C_4(PO)_3$ surfactant in the CO_2 huff-n-puff process, resulting in a 9.7%–13.2% increase in cumulative oil recovery from the reservoir matrix compared to the conventional CO_2 method. The modified process also enhanced the CO_2 storage capability in the reservoir, increasing it between 22.3% and 32.2% (Lv et al., 2023). Additionally, Hao et al. (2021) investigated the use of a stable N_2 foam to assist the CO_2 H-n-P process in heterogeneous edge-water reservoirs through mobility control, water-blocking mitigation, and improved oil contact. The results demonstrated that the foam-assisted process effectively mitigated water channeling and improved oil recovery compared to the conventional CO_2 H-n-P method (Hao et al., 2021).

In summary, this study's findings are consistent with current publications, which report higher oil recovery during the initial cycle of CO_2 H-n-P processes, followed by a decrease in effectiveness in subsequent cycles. This pattern underscores the importance of optimizing early cycles and considering reservoir characteristics to enhance overall recovery efficiency.

3.4. Characteristics of recoverable oil at the pore scale for different cycles of the CO_2 H-n-P injection process

The five CO_2 H-n-P injection process cycles can be divided into the early stage (cycles 1 and 2) and the late stage (cycles 3, 4, and 5). During the early stage, crude oil is primarily recovered from large and medium pores (macropores and mesopores), while oil from small pores (micropores) is gradually produced in the later stage. The sequence of oil produced in the pores during the CO_2 H-n-P process follows the order of large pores, then medium pores, and finally micropores. In contrast, the migration path of the crude oil produced is from micropores to mesopores, then to macropores.

Fig. 9 presents the NMR signal vs. pore size profiles for Core #1 during the CO_2 H-n-P injection process. The sequence of events includes initial oil saturation, the depleted development stage, and D_2O, followed by the first through fifth cycles of the H-n-P process. The pore size levels for micropores, mesopores, and macropores are marked in Fig. 8(a). Table 3 summarizes the total oil recovery and the contributions to oil recovery from different pore levels.

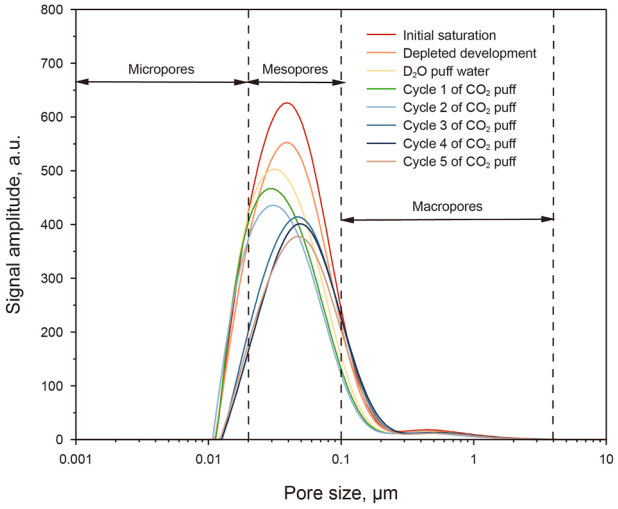

Fig. 9. Distribution of T_2 spectra of initial oil saturation, depleted development, water H-n-P (one cycle only), and each cycle of the CO_2 H-n-P injection process (Core #1).

As shown in Fig. 9 and Table 3, crude oil produced in cycle 1 of the CO_2 H-n-P process was primarily from mesopores, with a contribution efficiency of 66.42% compared to other pores. The lower pore utilization limit decreased by 27%, from 0.0267 to 0.0194 μm. In cycle 2, oil shifted predominantly to micropores, contributing 43.76%, which resulted in a decrease in recoverable oil in mesopores. The negative values in the macropores indicate that oil from other pore levels migrates to the macropores and is temporarily stored there during the "puff" process. These findings are consistent with the study by Xu et al. (2024).

Fig. 10(a) and (b) display the effluent produced during the water "puff" process and cycles 1 and 2 of the CO_2 "puff" process, along with the chromatographic analysis of the produced oil, respectively. During the water "puff" process, oil and water were observed to be produced from mesopores and macropores, while micropores did not contribute to oil recovery. Instead, some oil migrated to the smaller pores and was temporarily stored in situ. During cycles 1 and 2 of the CO_2 "puff" process, a small amount of water and a significant amount of oil were produced. This was due to the dissolution, swelling, and reduction of oil viscosity when CO_2 interacts with crude oil compared to the case of water "puff." The produced oil was analyzed using a chromatography method to determine its composition, and the results are presented in Fig. 10 (b).

Chromatographic analysis revealed that the composition of the produced crude oil remained consistent with that from the depletion development stage, indicating no significant change in oil components, as shown in Fig. 10(b). Expansion tests revealed that the CO_2 expansion coefficient in the target crude oil reached 1.16 at 32 MPa, resulting in a 19.4% decrease in viscosity. As a result of CO_2 dissolution, expansion, and viscosity reduction, the flow capacity of the oil phase was significantly improved.

The crude oil in micropores was primarily recovered during the third to fourth CO_2 H-n-P cycles, as shown in Table 3 and Fig. 9(b). No significant water phase backflow was observed, and the lower limit of pores contributing to oil production decreased from 0.019 to 0.0147 μm, as shown in Fig. 7. It was noted that the color of the produced oil phase gradually lightened, and the wall-hanging effect diminished. The proportion of light components (C_{14}–C_{20}) in the produced oil increased significantly, indicating a clear mass transfer of components, which chromatographic analysis revealed in Fig. 10(b). At this stage, the primary production mechanisms

Table 3
Oil recovery at the pore scale at different schemes for Core #1.

Sequence		Total oil recovery, %	Oil recovery from different types of pores, %		
			Micropores	Mesopores	Macropores
Depleted development scheme		11.78	3.88	6.72	1.18
Water (D_2O) scheme (one cycle)		8.12	−2.65	8.40	2.37
CO_2 H-n-P scheme	Cycle 1	6.67	1.37	4.43	0.87
	Cycle 2	3.68	2.34	1.61	−0.27
	Cycle 3	3.61	11.30	−3.85	−3.84
	Cycle 4	3.28	2.44	1.27	−0.43
	Cycle 5	3.08	−0.87	2.49	1.46

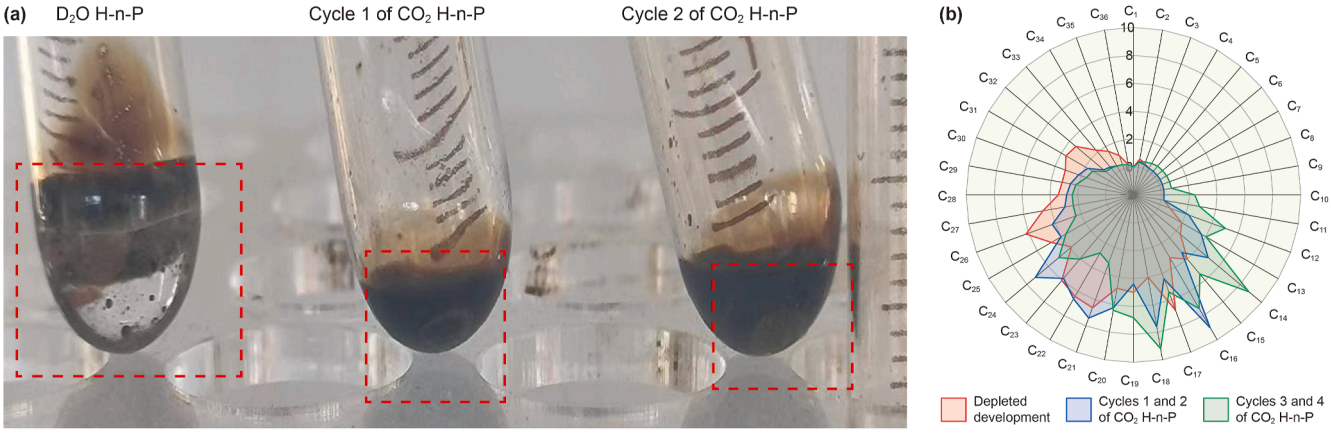

Fig. 10. Effluent from the core flooding experiment (**a**) and chromatographic analysis of components (**b**) with cycles of the CO_2 H-n-P injection process.

were component mass transfer and extraction, where lighter crude oil components were displaced from medium to large pores and subsequently produced.

3.5. Characteristics of the recoverable oil at the pore scale for different cycles of the HDC H-n-P injection process

Similar to the CO_2 H-n-P injection process, the HDC scheme was implemented following the depleted development stage and the water (D_2O) H-n-P injection process. Fig. 11 displays the NMR signal versus pore size profiles for Core #2 during the HDC H-n-P injection processes. The experiment progressed through initial oil saturation, depletion development, D_2O H-n-P injection, and five HDC H-n-P injection process cycles.

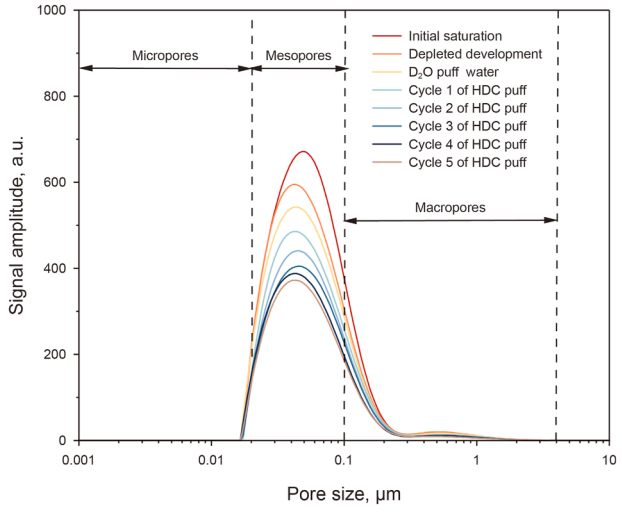

Fig. 11. Changes of T_2 spectrum with pore size for HDC H-n-P injection processes.

Fig. 11 illustrates that the lower limit of pore size utilization for oil recovery remains approximately 0.0281 μm, as shown in Fig. 8 (b) (Core #2), throughout the HDC H-n-P injection processes. The crude oil recovered in each cycle is primarily sourced from macropores and mesopores, leading to sustained oil production from large and medium-sized pores. Most oil is produced in the first two cycles, and no negative contribution from pore levels to oil recovery is observed in Table 4. This indicates that the HDC scheme effectively controls the oil flow dynamics at the pore scale. Table 4 summarizes the total oil recovery and the oil recovery contributions from different types of pores for Core #2.

Fig. 12(a) shows the viscosities of three cases: the original crude oil only, CO_2 and crude oil, and CO_2, viscosity reducer, and crude oil. Fig. 12(b) represents oil and water produced during the CO_2 and HDC H-n-P injection process. The oil samples produced during the tests were collected in a glass tube and are shown in Fig. 12(b). A similar performance was observed compared to the deleted development and D_2O stages. About 58.8% of the oil production contribution came primarily from mesopores in cycles 1 and 2 of the HDC H-n-P injection. The injection of oil-soluble viscosity reducer in cycles 1 and 2 effectively reduced the crude oil viscosity from 43.51 to 9.00 mPa·s, achieving a viscosity reduction capacity of 4.83 times under formation conditions. Thus, oil mobility and relative permeability are enhanced, resulting in increased oil production. In contrast, when CO_2 was injected into the core, the viscosity reduction was only 1.2 times, as shown in Fig. 12(a). Comparing the viscosity reduction effects of HDC and CO_2, HDC reduced viscosity four times more than CO_2. Regarding crude oil production over cycles 1 and 2, HDC yielded 3.48 times more oil from macropores, 1.64 times more from mesopores, and showed

Table 4
Oil recovery at the pore scale at different schemes for Core #2.

Sequence		Total oil recovery, %	Oil recovery from different types of pores, %		
			Micropores	Mesopores	Macropores
Depleted development scheme		10.94	0.23	8.73	1.98
Water (D_2O) H-n-P (one cycle only)		6.55	−1.13	6.07	1.61
HDC H-n-P scheme	Cycle 1	9.83	3.03	5.74	1.06
	Cycle 2	6.52	1.30	4.19	1.03
	Cycle 3	4.56	1.01	3.06	0.49
	Cycle 4	3.34	0.72	1.76	0.86
	Cycle 5	3.10	0.53	1.63	0.93

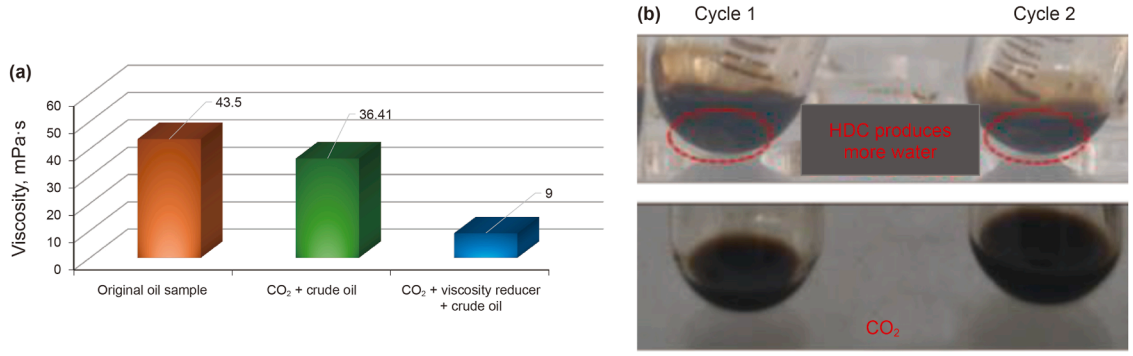

Fig. 12. Effect of HDC viscosity reduction (**a**) and effluent from online NMR core flooding experiment (**b**).

no significant difference from micropores compared to CO_2. In this scenario, there is a significant reduction in oil viscosity, enhanced fluidity, improved oil recovery, and increased flow-back efficiency of the aqueous phase. More water was produced in cycles 1 and 2 of the HDC H-n-P injection processes, as shown in Fig. 12(b). When comparing total oil recovery between the CO_2 and HDC cases, HDC demonstrated superior performance during the first three cycles. However, there was no significant difference in oil recovery between the two methods in cycles 4 and 5, as shown in Fig. 13.

The oil production performance in the later stage of HDC H-n-P injection processes is similar to that of CO_2 H-n-P injection processes. However, the extraction mechanism of recoverable oil in the formation differs completely. The viscosity reducers and light oil carriers were added to the crude oil phase, and the mass transfer of HDC–oil components weakened. Under residual oil saturation, the starting pressure of HDC is 1.58 times that of CO_2 (Fig. 14). It is difficult to produce crude oil from micropores in the later stage of the DHC H-n-P process, and the lower limit of pore size to produce recoverable oil is twice that of CO_2. As shown in Table 3 and Fig. 4, the oil recovery in macropores and mesopores was 5.09% and 6.54% higher than that of CO_2, respectively, but the recovery in micropores was 10.61% smaller than that of CO_2.

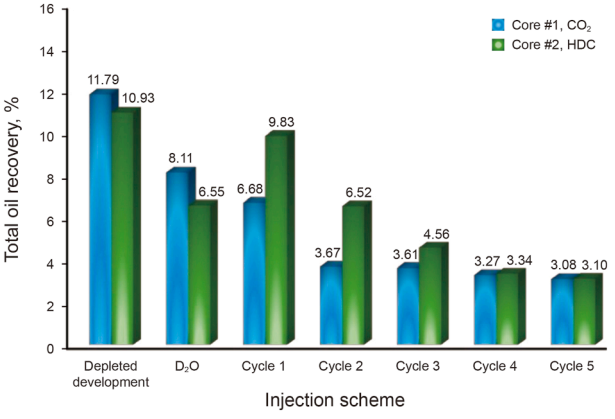

Fig. 13. Comparison of total oil recovery during the CO_2 and HDC H-n-P injection processes.

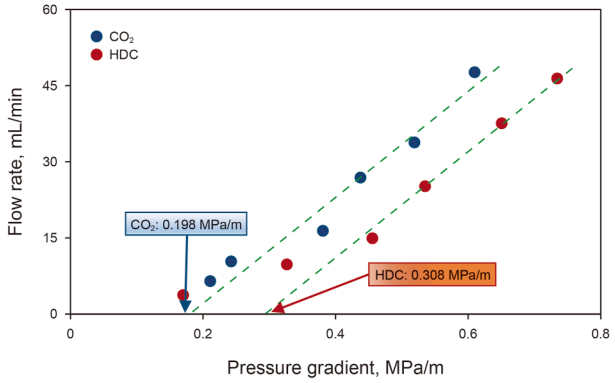

Fig. 14. Comparison of CO_2 and HDC start-up pressure gradients.

3.6. *Recoverable oil in the utilized zone flooded by water and its sweep efficiency during CO_2 and HDC H-n-P injection processes*

Figs. 9 and 11 present the NMR profiles showing pore size distribution for the CO_2 and HDC H-n-P injection processes. These charts determined the swept and non-swept areas during the water H-n-P injection process, as well as the pore and oil recovery contribution efficiencies from these areas, detailed in Tables 5 and 6, respectively. The core pore size is classified based on the minimum pore size required for recoverable oil during the CO_2 and D_2O H-n-P injection processes, which is that the lower limit of the pore utilization was 0.0267 μm for the CO_2 H-n-P and 0.0281 μm for the HDC case. The difference in the enclosed area in the NMR curve

Table 5
Comparison of swept and non-swept areas by water and pore contribution efficiency for CO_2 and HDC H-n-P injection processes.

Sequence	CO_2		HDC	
	Swept area by water, %	Non-swept area by water, %	Swept area by water, %	Non-swept area by water, %
Cycle 1	86.90	13.10	74.63	25.37
Cycle 2	82.96	17.04	87.71	12.29
Cycle 3	0	100	84.16	15.84
Cycle 4	42.57	57.43	87.42	12.58
Cycle 5	100.00	0	85.60	14.40

Table 6
Comparison of swept and non-swept areas by water and contribution efficiency of pore levels to oil recovery during CO_2 and HDC H-n-P injection processes.

Sequence	CO_2		HDC	
	Swept area by water, %	Non-swept area by water, %	Swept area by water, %	Non-swept area by water, %
Cycle 1	5.81	0.87	7.34	2.49
Cycle 2	3.04	0.63	5.72	0.80
Cycle 3	−4.05	7.66	3.84	0.72
Cycle 4	1.39	1.88	2.92	0.42
Cycle 5	3.93	−0.85	2.65	0.45
Total	10.12	10.19	22.47	4.88

before and after the injection process indicates the degree of pore utilization in that cycle. Multiple D_2O injection cycles categorize pores into water-swept and unswept areas for crude oil production, as shown in Fig. 15.

In the early stages of the H-n-P (cycles 1 and 2) of the CO_2 injection process, a significant amount of water in the pores obstructed CO_2 from contacting the crude oil. Due to water barriers, CO_2 does not improve crude oil mobility through dissolution, expansion, and viscosity reduction. However, HDC had a distinct advantage in reducing viscosity, accelerating water flow, draining oil, and achieving a better extraction effect (over 6%) than the CO_2 injection process. From cycles 3 to 5, the water shield effect significantly weakened. CO_2 gradually diffused into the oil, and mass transfer and pore extraction became the primary production mechanisms, with crude oil migrating to medium and large pores. Crude oil was recovered through HDC's synergistic viscosity reduction in water-flooded areas.

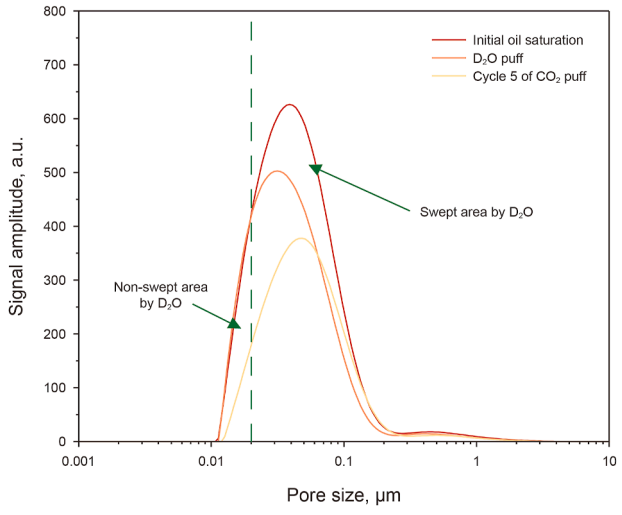

Fig. 15. Classification of swept and non-swept areas by water H-n-P injection process (lower limit of water utilization), following CO_2 H-n-P injection processes.

4. Study of CO_2 and HDC H-n-P technology through field case test

Using wells M56-7H, 72H, and 102H in the TH Oilfield as examples, five injection schemes were developed with a focus on cost control. The cost for a single H-n-P process was 1 million Chinese yuan, totaling 3 million Chinese yuan for three cycles. Viscosity reducer made up 1% by weight of the viscosity reduction system. Cost estimates were as follows: CO_2 at 500 Chinese yuan per ton, oil-soluble viscosity reducer at 67,000 Chinese yuan per ton, light oil carrier at 3800 Chinese yuan per ton, and the net profit from crude oil at 2666 Chinese yuan per ton.

A single-porosity model that accurately reflects its geological characteristics was developed using the GEM component simulator within the CMG numerical simulation software to investigate the enhanced oil recovery potential of a tight tuff heavy oil reservoir in the TH oilfield. This model was utilized to evaluate the impact of various injection strategies on oilfield recovery efficiency. The study designed and implemented five distinct injection schemes.

(1) Continuous injection of a single viscosity reducer during cycle 3 to improve fluidity by reducing crude oil viscosity.
(2) Single CO_2 injection during cycle 2 to promote oil recovery through CO_2 dissolution and expansion effects.
(3) Use of HDC during cycle 3 to reduce oil viscosity and assess its impact on enhanced oil recovery.
(4) A mixed injection strategy combining two cycles of HDC with one cycle of CO_2 injection to achieve a synergistic effect.
(5) One cycle of HDC combined with two cycles of single CO_2 injection to further explore the influence of different injection sequences on recovery.

Injection schemes 3 and 5 highlight the synergistic effect of HDC and CO_2 injection in improving oil recovery. Table 7 provides a detailed overview of all the injection schemes mentioned.

The GEM component simulator accurately conducted numerical simulations for the five injection schemes. The total oil production for each scheme was successfully modeled, with precise calculations of the oil change rate and input–output

Table 7
Comparison of the five injection schemes by numerical simulation for the field application.

Scheme number	Injection scheme	Material required	Total oil production, t	Oil change rate, t/t	Input–output ratio
1	Three cycles of pure viscosity reducer	214 t viscosity reducer per cycle	960	/	0.853
2	Three cycles of pure CO_2	2000 t CO_2 per cycle	1321	0.22	1.174
3	Three cycles of HDC	1500 t CO_2 + 60 t viscosity reducer per cycle	1526	0.34	1.356
4	Two cycles of HDC + one cycle of pure CO_2	Two cycles of 1500 t CO_2 + 60 t viscosity reducer and one cycle of 2000 t CO_2	1514	0.33	1.345
5	One cycle of HDC + two cycles of pure CO_2	One cycle of 1500 t CO_2 + 60 t viscosity reducer and two cycles of 2000 t CO_2	1531	0.28	1.361

ratio. All results are presented in Table 7. These simulation outcomes provide a clear production comparison and offer deeper insights into the mechanisms by which different injection schemes affect oilfield production dynamics, ultimate recovery, and economic performance. This research offers valuable theoretical and practical guidance for the development of the TH oilfield, as well as for other oilfields with similar geological conditions.

5. Future research directions

Since the laboratory study and field application of tight-tuff heavy oil reservoirs have just begun, few references exist, and many issues remain unclear. Several research gaps, operational challenges, and potential future research directions have been identified based on our knowledge of this reservoir type.

5.1. Research gaps and challenges

Using CO_2 as a displacing agent in tight-tuff heavy oil reservoirs and for in situ storage presents several research gaps that must be addressed to ensure enhanced recovery and long-term storage security. These gaps span from fundamental rock properties and fluid–mineral interactions to the challenges imposed by reservoir heterogeneity and caprock integrity. Tuff rocks from consolidated volcanic ash exhibit complex pore structures, variable mineral compositions, and cementation characteristics that differ significantly from conventional reservoirs. One key research gap is the limited understanding of how these unique properties influence CO_2 flow and displacement efficiency. For example, the distribution and connectivity of micro- and nanoscale pores in tuff rocks are poorly characterized, making it difficult to predict CO_2 transport and heavy oil mobilization. Moreover, the mechanical behavior of tuff under high-pressure CO_2 injection is not fully understood, especially in terms of fracture propagation and potential rock weakening. Addressing these uncertainties requires detailed pore-scale characterization and the development of predictive models that incorporate the specific textural and mineralogical attributes of tight-tuff formations.

Tuff formations often contain various clay minerals, which can interact with CO_2 in ways that impact oil recovery and reservoir stability. When CO_2 dissolves in formation water, it lowers the pH and potentially dissolves certain clay minerals. This may result in the precipitation of secondary minerals (scaling) and can clog pore throats, reducing permeability. Despite recognizing these processes, a research gap remains regarding the kinetics of these reactions under reservoir conditions and their long-term effects on both the displacement process and the formation's geomechanical properties. Comprehensive experimental studies and reactive transport modeling are needed to quantify these interactions and develop strategies to mitigate adverse effects.

The unique challenges with developing tight-tuff reservoirs are characterized by low porosity, low permeability, and complex pore structures. These reservoirs are significant due to their substantial hydrocarbon reserves, but technical and economic difficulties hinder their exploitation. Conventional extraction methods, such as water flooding, are ineffective due to the rock's tight nature, necessitating advanced techniques like CO_2 injection or hydraulic fracturing. The inherent heterogeneity in tight-tuff reservoirs is another major challenge. Variations in porosity, permeability, and mineralogy at different scales (from micro-fractures to macro-scale stratigraphic features) result in uneven fluid distribution. They can lead to early CO_2 breakthrough in the conventional continuous CO_2 injection mode. This heterogeneity complicates the prediction of sweep efficiency during CO_2 injection, as standard homogeneous reservoir models often fail to capture the complex flow pathways. Current research efforts are insufficient in providing robust upscaling techniques to integrate fine-scale heterogeneities into reservoir-scale simulations. Addressing this gap requires advanced imaging techniques, such as micro-CT and NMR imaging, combined with digital rock physics and multi-scale modeling, to better understand and predict fluid flow in these complex systems.

Operational challenges are also prominent. The low permeability of tight-tuff formations requires high injection pressures to achieve effective displacement, which increases the risk of formation damage if not carefully managed. Moreover, the complex interplay between mineral reactions and fluid dynamics may lead to early CO_2 breakthrough and uneven sweep efficiencies, thereby reducing overall recovery efficiency. The heavy oil in these reservoirs further complicates the recovery process, as its high viscosity may be difficult to overcome using conventional methods. Special experimental equipment is required to conduct core flooding tests at high temperatures and pressures.

Addressing these gaps and challenges will require a multidisciplinary approach that combines advanced experimental techniques, high-resolution imaging, reactive transport modeling, and field validation. Such efforts will be crucial for optimizing oil recovery processes and ensuring the safe, long-term storage of CO_2 in tight-tuff reservoirs.

5.2. Future research directions

Future research topics in the tight-tuff heavy oil reservoirs should focus on advanced pore-scale characterization, integrated modeling approaches, and mitigation of geochemical reactions.

5.2.1. Advanced pore-scale characterization

Advanced pore-scale characterization is crucial for understanding and optimizing oil recovery from tight-tuff rocks, which are characterized by extremely low permeability and complex pore networks. This approach integrates several state-of-the-art

imaging and analytical techniques to provide a comprehensive view of the rock's internal structure, pore connectivity, and mineral composition. One key technique is micro-computed tomography (micro-CT) scanning, which produces high-resolution three-dimensional images of the rock's pore network. Micro-CT enables the quantification of pore size distribution, the identification of pore throats, and the assessment of fracture networks at submicron scales. These detailed images enable researchers to visualize the spatial arrangement of pores and assess how structural heterogeneity affects fluid flow and recovery efficiency. In addition to micro-CT, scanning electron microscopy (SEM), often combined with energy-dispersive X-ray spectroscopy, examines the micro- and nano-scale mineralogical composition and surface textures. SEM-EDS analysis provides valuable insights into the diagenetic alterations, pore surface roughness, and the distribution of mineral phases within the tight-tuff matrix. This information is crucial for understanding how mineral heterogeneity and cementation influence the retention of fluids and the potential for undesirable reactions during enhanced oil recovery processes.

Another pivotal technique is nuclear magnetic resonance (NMR) imaging, which has evolved to include both static and dynamic (online) applications during core flooding experiments. Advanced NMR imaging enables real-time monitoring of fluid distribution, allowing for the distinction between bound and free fluids within the pore space. This capability is particularly valuable when assessing the performance of recovery processes, such as CO_2 H-n-P injections, continuous CO_2 injections, and water-alternating-CO_2 injections, as it provides quantitative measurements of oil saturation and pore utilization under dynamic conditions.

Overall, advanced pore-scale characterization for tight-tuff rocks offers an in-depth understanding of the intricate pore structures and mineralogical features that govern fluid dynamics. Such detailed insights are essential for designing optimized enhanced oil recovery strategies, mitigating issues related to low permeability, and ultimately improving the economic viability of tight-tuff reservoirs.

5.2.2. Integrated modeling approaches

Integrated modeling approaches for tight-tuff rocks involve a multi-scale and multi-physics framework that combines experimental data, advanced imaging techniques, and numerical simulations to predict reservoir behavior better and optimize enhanced oil recovery (EOR) strategies. The key components of the integrated modeling approach comprise pore-scale characterization and digital rock physics, upscaling to the reservoir scale, coupled multi-physics simulations, and calibration with experimental data. The modeling process should begin with detailed pore-scale characterization using techniques such as micro-computed tomography (micro-CT), scanning electron microscopy (SEM), and nuclear magnetic resonance (NMR) imaging. These techniques provide high-resolution data on pore geometry, connectivity, and mineralogy. This information is used to construct digital rock models that simulate fluid flow and reactive transport at the microscale, capturing the effects of heterogeneity and complex pore structures on permeability and recovery efficiency. The next step involves upscaling the detailed pore-scale models to create meso and macroscale reservoir models. Pore-network modeling and effective medium theories are typically employed to translate microscopic features into equivalent continuum properties that can be used in reservoir simulation. This integration bridges the gap between laboratory-scale observations and field-scale performance, enabling a more accurate prediction of fluid distribution and flow behavior across the reservoir. Thirdly, tight-tuff formations often experience complex interactions, including multiphase flow, geochemical reactions, and mechanical deformation. Integrated modeling approaches couple reactive transport simulations, which account for mineral dissolution, precipitation, and scaling, with geo-mechanical models that evaluate stress changes and fracture propagation. This comprehensive simulation framework enables the prediction of how injected fluids (such as CO_2 or viscosity reducers) interact with the rock matrix, thereby affecting recovery efficiency and long-term formation stability. Finally, core flooding experiments and laboratory tests validate the integrated models. These experiments, which simulate the injection of fluids under controlled conditions, yield data on pressure, saturation, and recovery performance. The experimental results are used to calibrate and refine the numerical models, ensuring that the simulations accurately reflect the behavior of tight-tuff reservoirs. Recent advances also incorporate machine learning techniques to optimize model parameters and improve predictive accuracy.

In summary, integrated modeling approaches for tight-tuff rocks combine advanced pore-scale characterization, upscaling techniques, coupled multi-physics simulations, and experimental calibration to provide a comprehensive understanding of reservoir behavior. This holistic strategy is essential for developing optimized EOR techniques that address the unique challenges posed by the complex geological and geochemical environments of tight-tuff formations. Comprehensive modeling should benefit from enhanced predictive capability, optimization of EOR strategies, and risk mitigation.

5.2.3. Mitigation of geochemical reactions

Mitigating geochemical reactions in tight-tuff rocks is critical for maintaining reservoir integrity and optimizing oil recovery. These reactions are related primarily to mineral dissolution and scaling (fine particle falloff and precipitation). This can alter the pore structure and permeability, reducing CO_2 injectivity and overall recovery efficiency. A comprehensive mitigation strategy encompasses both chemical and operational approaches, often supplemented by advanced predictive modeling. Controlling the pH, ionic strength, and concentration of key dissolved species in the injection water can significantly reduce aggressive reactions for chemical mitigation strategies. For instance, maintaining a near-neutral pH and minimizing high concentrations of ions such as sulfate and bicarbonate helps lower the risk of scaling and excessive mineral dissolution. Regarding chemical inhibitors, scale inhibitors, such as phosphonate-based compounds or specific polymers, can be added to the injection fluid to prevent the precipitation of mineral scales within pore throats. Additionally, corrosion inhibitors can be introduced to reduce metal leaching and subsequent mineral reactions that might compromise the rock matrix.

Another research direction to mitigate geochemical reactions may consider predictive modeling approaches. Integrated reactive transport modeling is crucial in mitigating geochemical reactions by forecasting the evolution of the reservoir's chemical environment under various injection scenarios. These models combine kinetic data for mineral dissolution and precipitation with reservoir flow dynamics to predict the extent and impact of geochemical interactions. The insights gained from such models are invaluable for designing injection strategies that minimize detrimental reactions while maximizing recovery efficiency.

5.2.4. Optimizing operational protocols and parameters

Optimizing operational protocols for tight-tuff heavy oil reservoirs is essential for enhancing oil recovery while minimizing formation damage, especially given the unique challenges posed by low permeability, complex pore networks, and geochemical reactivity. These protocols integrate tailored injection strategies,

real-time monitoring, and predictive modeling to adjust operational parameters and maximize recovery efficiency dynamically.

Tailored injection strategies: Tight-tuff reservoirs often require cyclic injection methods, such as the CO_2 H-n-P process, rather than continuous injection. In this approach, the injection phase involves carefully increasing the pressure to the reservoir level at a controlled rate to avoid inducing fractures or exacerbating geochemical reactions. This is followed by a soaking period that allows the injected CO_2 or enhanced fluids to interact with the heavy oil, reducing viscosity and facilitating mobilization. Finally, the production phase is initiated from the same injection well to recover the mobilized oil. The duration of each phase is optimized based on reservoir properties and laboratory core flooding experiments.

Real-time monitoring and adaptive control: Continuous monitoring is critical given the dynamic conditions within tight-tuff formations. Advanced technologies, including pressure sensors and online NMR imaging, are utilized to monitor real-time changes in pressure, temperature, and fluid saturation. This real-time data enables operators to adjust injection rates, pressures, and fluid compositions, thereby mitigating issues such as early CO_2 breakthroughs or adverse geochemical reactions.

Operational flexibility and continuous improvement: The protocols also emphasize operational flexibility by combining real-time monitoring with predictive simulation, allowing operators to implement adaptive management strategies that continuously refine injection and production schedules. This iterative process not only enhances oil recovery efficiency but also extends the operational life of the reservoir by preventing irreversible formation damage.

Optimizing operational protocols for tight-tuff heavy oil reservoirs is built on tailored cyclic injection strategies, real-time monitoring systems, and integrated predictive modeling. Together, these components allow precise control over the injection process, enabling operators to adjust to changing reservoir conditions, mitigate adverse geochemical reactions, and maximize oil recovery while preserving reservoir integrity.

6. Conclusions

Based on the experimental results of online NMR core flooding experiments, including the depleted development, CO_2, and HDC H-n-P injection processes for low-permeability cores and fluids under reservoir conditions, the following conclusions can be drawn.

(1) The TH tight sedimentary tuff heavy oil reservoir is characterized by medium to high porosity, ultra-low permeability, and a small average pore throat radius. Additionally, crude oil has a high viscosity, significantly contributing to poor fluid mobility and suboptimal development outcomes. The high compressibility coefficient of the reservoir favors depleted development and H-n-P processes, relying on elastic energy. Over 85% of the crude oil produced comes from macropores and mesopores, with the minimum pore size utilized for oil production being above 0.02 μm.

(2) During the five CO_2 H-n-P cycles, oil is recovered from macropores, mesopores, and micropores as CO_2 displaces oil and water, gradually extending the lower pore size limit. In the early cycles, CO_2 targets larger pores, displacing fluids through dissolution, expansion, and viscosity reduction, with 85% of oil recovery from the aqueous phase. As the water shield weakens in later cycles, CO_2 reaches micropores for further oil extraction. The lower pore size limit decreases with more CO_2 cycles.

(3) Viscosity reduction plays a key role in the extraction mechanism during multiple cycles of the HDC H-n-P injection process, with over 80% of the oil recovery attributed to the area coming from the swept zone by water. In the early stages, oil recovery was 6.38% higher than the CO_2 H-n-P process, while the later recovery rates became similar to those of CO_2. However, the extraction mechanisms and production patterns of the two methods differed notably.

(4) The viscosity reduction rate of HDC agents at a 9:1 ratio is 4.85 times higher than that of CO_2. Crude oil in the mesopores and macropores within the water-injected zone can be further recoverable, mitigating the damage caused by heavy component deposition during the later stages of the H-n-P process. However, the slightly lower injectivity of HDC compared to CO_2 reduces its mass transfer and extraction efficiency when using light oil as a carrier, leading to an increase in the lower limit for pore size utilized (~0.03 μm). As a result, it becomes challenging to recover crude oil from micropores.

(5) Given certain investment conditions, the recommended injection plan for the target block is one cycle of HDC H-n-P injection followed by two cycles of CO_2 H-n-P injection.

CRediT authorship contribution statement

Hao Chen: Writing – original draft. **Pei-Fu Xu:** Writing – review & editing, Data curation. **Yong-Xian Zhu:** Investigation. **Jia-Yi Yu:** Investigation. **Mei Zhang:** Investigation. **Xian-Min Zhou:** Methodology, Conceptualization. **Ming-Cheng Ni:** Investigation. **Yi Wu:** Data curation. **Xi-Liang Liu:** Data curation.

Data availability

Data will be made available on request.

Declaration of competing interest

The authors declare that they have no known competing financial interests or personal relationships that could have appeared to influence the work reported in this manuscript.

Acknowledgments

This study has been funded by the Natural Science Foundation of Beijing Municipality (3232028) , the National Natural Science Foundation of China (52274053) and the National Foreign Expert Individual Project (H20240045). Moreover, we would like to express our heartfelt appreciation to the CMG-CUP Joint Numerical Reservoir Simulation Laboratory, which provided the free CMG reservoir simulation software used in this research.

References

Alcalde, J., Heinemann, N., James, A., Bond, C.E., Ghanbari, S., Mackay, E.J., Haszeldine, R.S., Faulkner, D.R., Worden, R.H., Allen, M.J., 2021. A criteria-driven approach to the CO_2 storage site selection of East Mey for the acorn project in the North Sea. Mar. Petrol. Geol. 133, 105309. https://doi.org/10.1016/j.marpetgeo.2021.105309.

Bank, G.C., Riestenberg, D.E., Koperna, G.J., 2007. CO_2-enhanced oil recovery potential of the Appalachian Basin. In: Eastern Regional Meeting. https://doi.org/10.2118/111282-MS.

Cao, M., Gu, Y., 2013. Physicochemical characterization of produced oils and gases in immiscible and miscible CO_2 flooding processes. Energy & Fuel. 27 (1), 440–453. https://doi.org/10.1021/ef301407k.

Chen, T., Yang, Z., Ding, Y., Luo, Y., Qi, D., Lin, W., Zhao, X., 2018. Waterflooding huff-n-puff in tight oil cores using online nuclear magnetic resonance. Energies 11 (6), 1524. https://doi.org/10.3390/en11061524.

Chen, Y., Sari, A., Xie, Q., Saeedi, A., 2019. Excess H^+ increases hydrophilicity during CO_2-assisted enhanced oil recovery in sandstone reservoirs. Energy & Fuel 33 (2), 814–821. https://doi.org/10.1021/acs.energyfuels.8b03573.

Davoodi, S., Al-Shargabi, M., Wood, D.A., Mehrad, M., Rukavishnikov, V.S., 2024. Carbon dioxide sequestration through enhanced oil recovery: A review of storage mechanisms and technological applications. Fuel 366, 131313. https://doi.org/10.1016/j.fuel.2024.131313.

Du, M., Yang, Z., Feng, C., Yao, L., Chen, X., Li, H., 2023. Microscopic production characteristics of pore crude oil and influencing factors during enhanced oil recovery by air injection in shale oil reservoirs. ACS Omega 8 (20), 18186–18201. https://doi.org/10.1021/acsomega.3c01585.

Gong, G., Sun, B., Liu, M., Ye, C., Gao, B., 2006. NMR relaxation of the fluid in rock porous media. Chin. J. Magn. Reson. 23 (3), 379–395. https://doi.org/10.3969/j.issn.1000-3290.2001.03.001 (in Chinese).

Hao, H., Hou, J., Zhao, F., Huang, H., Liu, H., 2021. N_2-foam-assisted CO_2 huff-n-puff process for enhanced oil recovery in a heterogeneous edge-water reservoir: Experiments and pilot tests. RSC Adv. 11 (2), 1134–1146. https://doi.org/10.1039/d0ra09448j.

Hao, H., Yuan, D., Hou, J., Guo, W., Liu, H., 2022. Using starch graft copolymer gel to assist the CO_2 huff-n-puff process for enhanced oil recovery in a water channeling reservoir. RSC Adv. 12 (31), 19990–20003. https://doi.org/10.1039/d2ra01812h.

He, Y., Cheng, S., Sun, Z., Chai, Z., Rui, Z., 2020. Improving oil recovery through fracture injection and production of multiple fractured horizontal wells. J. Energy Resour. Technol. 142 (5), 53–62. https://doi.org/10.1115/1.4045957.

Hou, W., Zhao, T., Zhang, L., Xiong, C., Xu, H., Chao, H., Zhang, W., Wang, W., Zhang, h., 2020. Stress sensitivity and prediction of irreducible water saturation in coal reservoirs in Baode and Hancheng blocks based on low-field nuclear magnetic resonance. J. Jilin Univ. (Earth Sci. Ed.) 50 (2), 608–616. https://doi.org/10.13278/j.cnki.jjuese.20190252 (in Chinese).

Huang, X., Li, X., Zhang, Y., et al., 2022. Microscopic production characteristics of crude oil in nano-pores of shale oil reservoirs during CO_2 huff and puff. Petrol. Explor. Dev. 49 (3), 636–643. https://doi.org/10.1016/S1876-3804(22)60053-3.

Huang, Z., Zhao, Q., Chen, L., Guo, L., Miao, Y., Wang, Y., Jin, H., 2023. Experimental investigation of enhanced oil recovery and in-situ upgrading of heavy oil via CO_2- and N_2-assisted supercritical water flooding. Chem. Eng. Sci. 268, 118378. https://doi.org/10.1016/j.ces.2022.118378.

Jia, Y., 2019. Evaluation on carbon dioxide huff and puff effect and analysis of its influencing factors in Qikeshu oilfield. Adv. Fine Petrochem. 20, 15–18. https://doi.org/10.13534/j.cnki.32-1601/te.2019.04.005.

Kumar, N., Sampaio, M.A., Ojha, K., Hoteit, H., Mandal, A., 2022. Fundamental aspects, mechanisms, and emerging possibilities of CO_2 miscible flooding in enhanced oil recovery: A review. Fuel 330, 125633. https://doi.org/10.1016/j.fuel.2022.125633.

Li, A., Ren, X., Wang, G., Wang, Y., Jiang, K., 2015. Characterization of pore structure of low permeability reservoirs using a nuclear magnetic resonance method. J. China Univ. Pet. (Ed. Nat. Sci.) 39 (6), 92–98. https://doi.org/10.3696/j.issn.1673-5005.2015.06.012 (in Chinese).

Li, D., Saraji, D., Jiao, S., Zhang, Z., 2021. CO_2 injection strategies for enhanced oil recovery and geological sequestration in a tight reservoir: An experimental study. Fuel 284, 119013. https://doi.org/10.1016/j.petrol.2020.108247.

Li, J., Wang, M., Fei, J., Xu, L., Shao, H., Li, M., Tian, W., Lu, S., 2022. Determination of in situ hydrocarbon contents in shale oil plays. Part 2: Two-dimensional nuclear magnetic resonance (2D NMR) as a potential approach to characterize preserved cores. Mar. Petrol. Geol. 145, 105890. https://doi.org/10.1016/j.marpetgeo.2022.105890.

Li, J.B., Wang, M., Shao, H.M., Li, M., Liu, L., Lu, S.F., 2023. Shale porosity measurement by the saturated oil method: Removing the contribution from oils dissolved in kerogen. Pet. Sci. 20, 3273–3279. https://doi.org/10.1016/j.petsci.2023.07.006.

Li, S., Zhu, J., Wang, Z., Li, M., Wei, Y., Zhang, K., 2024. Chemical strategies for enhancing CO_2-hydrocarbon miscibility. Sep. Purif. Technol. 337, 126436. https://doi.org/10.1016/j.seppur.2024.126436.

Li, Z., Qu, X., Liu, W., et al., 2015. Development modes of Triassic Yanchang Formation Chang Member tight oil in Ordos Basin, NW China. Petrol. Explor. Dev. 42, 217–221. https://doi.org/10.11698/PED.2015.02.11 (in Chinese).

Liang, S., Luo, Q., Wang, R., et al., 2019. Geological characteristics and exploration practice of unconventional Permian oil resources in Santanghu Basin. China Pet. Explor. 24, 624–635. https://doi.org/10.3969/J.ISSN.1672-7703.2019.05.009 (in Chinese).

Liu, B., Lei, X., Feng, D., Ahmadi, M., Wei, Z., Chen, Z., Jiang, L., 2025. Nanoconfinement effect on the miscible behaviors of CO_2/shale oil/surfactant systems in nanopores: Implications for CO_2 sequestration and enhanced oil recovery. Sep. Purif. Technol. 356 (A), 129826. https://doi.org/10.1016/j.seppur.2024.129826.

Liu, W., Du, L., Zou, X., Liu, T., Wu, X., Wang, Y., Dong, J., 2023. Experimental study on the enhanced ultra-heavy oil recovery using an oil-soluble viscosity reducer and CO_2 assisted steam flooding. Geoenergy Sci. Eng. 222, 211409. https://doi.org/10.1016/j.geoen.2022.211409.

Lu, H., Wang, Z., Peng, T., Zheng, J., Yang, X., Qin, X., 2021. A novel method for improving recovery of heavy oil reservoirs with high water cut based on polymer gel-assisted CO_2 huff and puff. J. Pet. Explor. Prod. Technol. 11, 3533–3541. https://doi.org/10.1007/s13202-021-01232-z.

Lu, M., Qin, Q., Zhong, A., Zhang, Z., Zhang, L., 2024. Investigation on the flow behavior and mechanisms of water flooding and CO_2 immiscible/miscible flooding in shale oil reservoirs. J. CO_2 Util. 80, 102660. https://doi.org/10.1016/j.jcou.2023.102660.

Lu, Y., Liu, K., Wang, Y., 2021. Applying NMR T_2 spectral parameters in pore structure evaluation—An example from an eocene low-permeability sandstone reservoir. Appl. Sci. 11, 8027. https://doi.org/10.3390/app11178027.

Luo, Y., Zheng, T., Xiao, H., Liu, X., Zhang, H., Wu, Z., Zhao, X., Xia, D., 2022. Identification of distinctions of immiscible CO_2 huff and puff performance in Chang-7 tight sandstone oil reservoir by applying NMR, microscope, and reservoir simulation. J. Petrol. Sci. Eng. 209, 109719. https://doi.org/10.1016/j.petrol.2021.109719.

Luo, Y., Liu, X., Xiao, H., Zheng, T., 2023a. Microscopic production characteristics of tight oil in the nanopores of different CO_2-affected areas from molecular dynamics simulations. Sep. Purif. Technol. 306 (A), 122607. https://doi.org/10.1016/S1876-3804(22)60053-3.

Luo, Y., Xiao, H., Liu, X., Zheng, T., Wu, Z., 2023b. Diffusion coefficient and the volume swelling of CO_2/light oil systems: Insights from dynamic volume analysis and molecular dynamics simulation. J. Mol. Liq. 382, 121943. https://doi.org/10.1016/j.molliq.2023.121943.

Lv, Q., Zheng, R., Guo, X., Larestani, A., Hadavimoghaddam, F., Riazi, M., Hemmati-Sarapardeh, A., Wang, K., Li, J., 2023. Modeling minimum miscibility pressure of CO_2-crude oil systems using deep learning, tree-based, and thermodynamic models: Application to CO_2 sequestration and enhanced oil recovery. Sep. Purif. Technol. 310, 123086. https://doi.org/10.1016/j.seppur.2022.123086.

Lv, W., Gong, H., Dong, M., Li, Y., Sun, H., Sun, Z., Jiang, H., 2024. Potential of nonionic polyether surfactant-assisted CO_2 huff-n-puff for enhanced oil recovery and CO_2 storage in ultra-low permeability unconventional reservoirs. Fuel 359, 130474. https://doi.org/10.1016/j.fuel.2023.130474.

Monger, T.G., Coma, J.M., 1988. A laboratory and field evaluation of the CO_2 huff 'n' puff process for light-oil recovery. SPE Reserv. Eng. 3 (4), 1168–1176. https://doi.org/10.2118/15501-PA.

Moultos, I.N., Tsimpanogiannis, Panagiotopoulos A.Z., Economou, I.G., 2016. Self-diffusion coefficients of the binary (H_2O+CO_2) mixture at high temperatures and pressures. J. Chem. Thermodyn. 93, 424–429. https://doi.org/10.1016/j.jct.2015.04.007.

Or, C., Sasaki, K., Sugai, Y., Nakano, M., Imai, M., 2016. Swelling and viscosity reduction of heavy oil by CO_2-gas foaming in immiscible condition. SPE Reservoir Eval. Eng. 19 (2), 294–304. https://doi.org/10.2118/179738-PA.

Ordorica-Garcia, G., Elkamel, A., Douglas, P., Croiset, E., Gupta, M., 2009. Optimizing energy production with integrated CCS technology for CO_2 emissions mitigation in the Canadian oil sands industry. Energy Proc. 1, 3985–3992. https://doi.org/10.1016/j.egypro.2009.02.203.

Ozkan, S., Kurtoglu, B., Ozkan, E., 2012. Long-term economic viability of production from unconventional liquids-rich reservoirs: The case of Bakken field. SPE Econ. Manag. 4 (4), 215–221. https://doi.org/10.2118/162901-PA.

Ren, S., Aldahri, T., Liu, W., Liang, B., Lund, H., Kaiser, M.J., 2021. CO_2 mineral sequestration by using blast furnace slag: From batch to continuous experiments. Energy 214. https://doi.org/10.1016/j.energy.2020.118975.

Rylander, E., Philip, M.S., Jiang, T., Lewis, R., 2013. NMR T_2 distributions in the Eagle Ford Shale: Reflections on pore size. In: SPE Unconventional Resources Conference/Gas Technology Symposium. https://doi.org/10.2118/164554-MS.

Sahu, C., Prasad, S.K., Kumar, R., Sangwai, J.S., 2023. High-pressure rheological signatures of CO_2 hydrate slurries formed from gaseous and liquid CO_2 relevant for refrigeration, pipeline transportation, carbon capture, and geological sequestration. Sep. Purif. Technol. 309, 123087. https://doi.org/10.1016/j.seppur.2022.123087.

Sayegh, S.G., Maini, B.B., 1984. Laboratory evaluation of the CO_2 huff-n-puff process for heavy oil reservoirs. J. Can. Petrol. Technol. 23 (3). https://doi.org/10.2118/84-03-02.

Shi, Y., Wu, B., Wang, H., Li, Y., Liu, Z., Xu, C., Qin, J., Li, Y., Song, Z., Liu, H., 2024. Insights into CO_2 huff-n-puff mechanisms from laboratory experiment and single-well pilot test in the Lucaogou tight oil reservoir, Jimsar sag, China. Geoenergy Sci. Eng. 232 (B), 212456. https://doi.org/10.1016/j.geoen.2023.212456.

Song, Z., Song, Y., Li, Y., Bai, B., Hou, J., 2020. A critical review of CO_2 enhanced oil recovery in tight oil reservoirs of North America and China. Fuel 276, 118006. https://doi.org/10.1016/j.fuel.2020.118006.

Sun, S., Liang, S., Liu, Y., Liu, D., Gao, M., Tian, Y., Wang, J., 2023. A review on shale oil and gas characteristics and molecular dynamics simulation for the fluid behavior in shale pores. J. Mol. Liq. 376, 121507. https://doi.org/10.1016/j.molliq.2023.121507.

Tang, J., Zhang, M., Guo, X., Geng, J., Li, Y., 2024. Investigation of creep and transport mechanisms of CO_2 fracturing within natural gas hydrates. Energy 300, 131214. https://doi.org/10.1016/j.energy.2024.131214.

Tang, W.-Y., Sheng, J.J., Jiang, T.-X., 2023. Further discussion of CO_2 huff-n-puff mechanisms in tight oil reservoirs based on NMR monitored fluids spatial distributions. Pet. Sci. 20 (1), 350–361. https://doi.org/10.1016/j.petsci.2022.08.014.

Tao, L., Chen, Y., Liu, N., Wu, D., Meng, S., Li, S., Yang, Y., 2022. A novel experimental method for the evaluation of residual oil distribution in a sand-packed model by using nitrogen and viscosity reducer huff-puff technology to develop heavy oil reservoirs. J. Petrol. Sci. Eng. 208 (C), 109585. https://doi.org/10.1016/j.petrol.2021.109585.

Timur, A., 1969. Pulsed nuclear magnetic resonance studies of porosity, movable fluid, and permeability of sandstones. J. Petrol. Technol. 21 (6), 775. https://doi.org/10.2118/2045-PA.

Wang, L., Zhang, Y., Zou, R., Zou, R., Huang, L., Liu, L., Meng, Z., Wang, Z., Lei, H., 2023. A systematic review of CO_2 injection for enhanced oil recovery and carbon storage in shale reservoirs. Int. J. Hydrogen Energy 48, 37134–37165. https://doi.org/10.1016/j.ijhydene.2023.06.099.

Wang, L., Zhang, Y., Zou, R., Zou, R., Yuan, Y., Huang, L., Liu, Y., Meng, Z., 2025. Dynamics of oil–CO_2–water three-phase under the nanopore confinement effect: Implications for CO_2 enhanced shale oil recovery and carbon storage. Sep. Purif. Technol. 354 (3), 128892. https://doi.org/10.1016/j.seppur.2024.128892.

Wang, T., Wang, L., Meng, X., Chen, Y., Song, W., Yuan, C., 2023. Key parameters and dominant EOR mechanism of CO_2 miscible flooding applied in low-permeability oil reservoirs. Geoenergy Sci. Eng. 225, 211724. https://doi.org/10.1016/j.geoen.2023.211724.

Wang, Y., Gao, H., Li, X., 2021. Study of water huff-n-puff in low-permeability oil reservoirs. Front. Earth Sci. 9, 824410. https://doi.org/10.3389/feart.2021.824410.

Wei, B., Gao, K., Song, T., Zhang, X., Pu, W., Xu, X., Wood, C., 2020. Nuclear-magnetic resonance monitoring of mass exchange in a low-permeability matrix/fracture model during CO_2 cyclic injection: A mechanistic study. SPE J. 25 (1), 440–450. https://doi.org/10.2118/199345-PA.

Wu, S., Li, Z., Sarma, H.K., 2020. Influence of confinement effect on recovery mechanisms of CO_2-enhanced tight-oil recovery process considering critical properties shift, capillarity, and adsorption. Fuel 262, 116569. https://doi.org/10.1016/j.fuel.2019.116569.

Wu, Y., Li, P., Yan, B., Li, X., Huang, Y., Yuan, J., Feng C., X., 2024. A salt-induced tackifying polymer for enhancing oil recovery in high salinity reservoirs: Synthesis, evaluation, and mechanism. Green Energy Environ. 9 (11), 1747–1758. https://doi.org/10.1016/j.gee.2023.10.006.

Xia, Z., Yin, H., Wang, X., Xu, G., 2024. Surfactant slug assisting CO_2 huff and puff in enhancing shale oil reservoir recovery. Phys. Fluids 36 (1). https://doi.org/10.1063/5.0185454.

Xu, L., Li, Q., Myers, M., Tan, Y., He, M., Umeobi, H.I., Li, X., 2021. The effects of porosity and permeability changes on simulated supercritical CO_2 migration front in tight glutenite under different effective confining pressures from 1.5 MPa to 21.5 MPa. Greenhouse Gases: Sci. Technol. 11, 19–36. https://doi.org/10.1002/ghg.2043.

Xu, T., Wang, J., Lu, Y., et al., 2024. Exploring pore-scale production characteristics of oil shale after CO_2 huff'n'puff in fractured shale with varied permeability. Int. J. Coal Sci. Technol. 11. https://doi.org/10.1007/s40789-024-00664-2.

Xu, Z., Li, Z., Liu, Z., Li, B., Zhang, Q., Zheng, L., Song, Y., Husein, M.M., 2022. Characteristics of CO_2 foam plugging and migration: Implications for geological carbon storage and utilization in fractured reservoirs. Sep. Purif. Technol. 294, 121190. https://doi.org/10.1016/j.seppur.2022.121190.

Yan, X., Li, B., Li, Z., Li, Z., Wang, B., Wang, X., Zhang, M., Li, W., 2025. Gas channeling control with CO_2-responsive gel system in fractured low-permeability reservoirs: Enhancing oil recovery during CO_2 flooding. Sep. Purif. Technol. 353 (B), 128475. https://doi.org/10.1016/j.seppur.2024.128475.

Yu, J., Li, D., He, B., et al., 2020. Effective development technology of tight oil in sedimentary tuff of Tiaohu Formation in Santanghu Basin. Xinjing Pet. Geol. 41, 714–720. https://doi.org/10.7657/XJPG20200612 (in Chinese).

Zhang, D., Li, L., Wang, H., Su, Y., Zhang, X., Zheng, N., Huang, Z., Yao, C., 2023. Study on the mechanism of CO_2 huff-n-puff enhanced oil recovery and storage in shale porous media considering heterogeneous structure. Phys. Fluids 36 (7), 072005. https://doi.org/10.1063/5.0210933.

Zhang, Y., Li, Y., Li, X., 2019. Advances in tight oil reservoir development: A review of CO_2 huff and puff. Adv. Geo-Energy Res. 4 (3), 280–289. https://doi.org/10.46690/ager.2019.03.02.

Zhao, F., Zhu, H., Cui, Q., Wang, B.H., Zhang, Y., 2021. Anaerobic production of surfactin by a new *Bacillus subtilis* isolate and the in situ emulsification and viscosity reduction effect towards enhanced oil recovery applications. J. Petrol. Sci. Eng. 201, 108508. https://doi.org/10.1016/j.petrol.2021.108508.

Zhao, J., Yang, L., Yang, D., Kang, Z., Wang, L., 2022. Study on pore and fracture evolution characteristics of oil shale pyrolysed by high-temperature water vapour. Oil Shale 39 (1), 79–95. https://doi.org/10.3176/oil.2022.1.05.

Zhou, X., Wu, Y.S., Chen, H., Elsayed, M., Yu, W., Zhao, X., Murtaza, M., Kamal, M.S., Sarmad Khan, Z., Al-Abdrabalnabi, R., Bo, Ren B., 2024a. Review of carbon dioxide utilization and sequestration in depleted oil reservoirs. Renew. Sustain. Energy Rev. 202, 114646. https://doi.org/10.1016/j.rser.2024.114646.

Zhou, X., Yu, W., Lei, G., Khan, S.Z., Al-Abdrabainabi, R., Kamal, M.S., Wu, Y.S., 2024b. Experimental study on dual benefits of improvement of CO_2 enhanced oil recovery and its storage capacity for depleted carbonate oil reservoirs. Adv. Geo-Energy Res. 12 (1), 52–65. https://doi.org/10.46690/ager.2024.04.05.